



Published in final edited form as:

Structure. 2022 September 01; 30(9): 1269–1284.e6. doi:10.1016/j.str.2022.05.017.

## Cullin-independent recognition of HHARI substrates by a dynamic RBR catalytic domain

Katherine H Reiter<sup>1,4</sup>, Alex Zelter<sup>1</sup>, Maria K Janowska<sup>1</sup>, Michael Riffle<sup>1</sup>, Nicholas Shulman<sup>2</sup>, Brendan X. MacLean<sup>2</sup>, Kaipo Tamura<sup>2</sup>, Matthew C Chambers<sup>2</sup>, Michael J MacCoss<sup>2</sup>, Trisha N Davis<sup>1</sup>, Miklos Guttman<sup>3</sup>, Peter S Brzovic<sup>1</sup>, Rachel E Klevit<sup>1,5,\*</sup>

<sup>1</sup>Department of Biochemistry, University of Washington, Seattle, WA 98195, USA

<sup>2</sup>Department of Genome Sciences, University of Washington, Seattle, WA 98195, USA

<sup>3</sup>Department of Medicinal Chemistry, University of Washington, Seattle, WA 98195, USA

<sup>4</sup>Present address: Center for Development of Therapeutics, Broad Institute, Cambridge, MA 02142, USA

<sup>5</sup>Lead Contact

### SUMMARY

RING-Between-RING (RBR) E3 ligases mediate ubiquitin transfer through an obligate E3-ubiquitin thioester intermediate prior to substrate ubiquitination. While RBRs share a conserved catalytic module, substrate recruitment mechanisms remain enigmatic and the relevant domains have yet to be identified for any member of the class. Here we characterize the interaction between the auto-inhibited RBR, HHARI (AriH1), and its target protein, 4EHP, using a combination of XL-MS, HDX-MS, NMR, and biochemical studies. The results show that 1) a di-aromatic surface on the catalytic HHARI Rcat domain forms a binding platform for substrates and 2) a phosphomimetic mutation on the auto-inhibitory Ariadne domain of HHARI promotes release and reorientation of Rcat for transthiolation and substrate modification. The findings identify a direct binding interaction between a RING-Between-RING ligase and its substrate and suggest a general model for RBR substrate recognition.

### Graphical Abstract

\*Correspondence: Rachel E Klevit (klevit@uw.edu).

Author Contributions: K.H.R., A.Z., M.K.J., and R.E.K. conceived the project, designed the experiments, and analyzed data. A.Z. designed the XL-MS experiments. XL-MS data analysis was by A.Z. and K.H.R. M.R. developed ProXL. N.S., B.X.M., K.T., and M.C.C. wrote software for quantification of XL peptides in Skyline. K.H.R. performed HDX-MS experiments under the supervision of M.G. M.K.J. wrote HDXBoxeR, an R-package for statistical analysis of HDX-MS data. K.H.R. conducted and analyzed NMR experiments under the guidance of P.S.B. K.H.R. generated docking models. K.H.R. purified proteins, performed assays, and analyzed data. The manuscript was written by K.H.R. and R.E.K. with input from all co-authors.

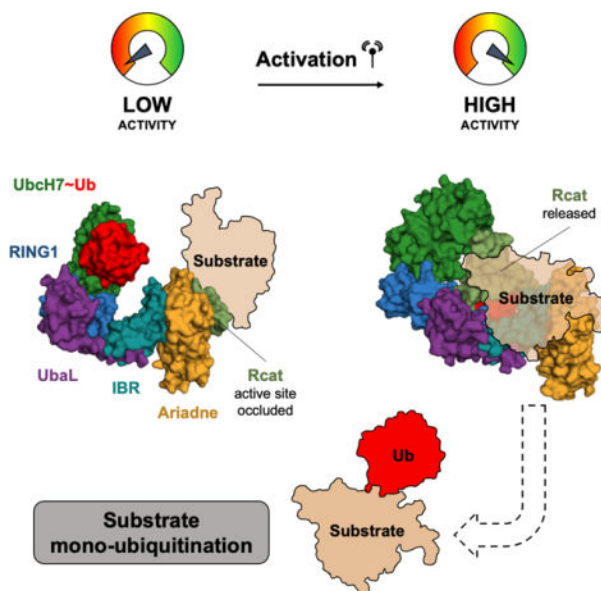
**Publisher's Disclaimer:** This is a PDF file of an unedited manuscript that has been accepted for publication. As a service to our customers we are providing this early version of the manuscript. The manuscript will undergo copyediting, typesetting, and review of the resulting proof before it is published in its final form. Please note that during the production process errors may be discovered which could affect the content, and all legal disclaimers that apply to the journal pertain.

Declarations of Interest

The authors declare no competing interests.

Supplemental Items

Supplementary Table 2 HDXMS Summary, related to Figures 4–6, S4



## ETOC Blurp

HHARI is an auto-inhibited RING-Between-RING ubiquitin ligase involved in genotoxic stress, signaling, and organogenesis. Reiter et al use integrated structural approaches to monitor the conformational response of HHARI upon activation and substrate binding, revealing a non-ubiquitin substrate binding platform in the HHARI Rcat domain.

## INTRODUCTION

Covalent modification of proteins by ubiquitin (Ub) is a fundamental biological signal involved in nearly all eukaryotic cellular processes. A highly varied and complicated Ub code is generated through serial action of three enzymes (E1, E2, and E3) that require tight regulation to ensure accurate execution of the signal. Attachment of single or multiple Ub moieties (mono- vs. poly-ubiquitylation) are distinct outcomes that direct a substrate's fate, dictating proteasomal degradation of the target, changes in protein-protein interactions, altered function, or protection from other post-translational modifications (Swatek and Komander, 2016). Specific outcomes require careful targeting of substrates by E3s to avoid potential pathological effects associated with cancer, neurodegeneration, and developmental disorders. Consequently, there is great interest in substrate recognition and ubiquitin transfer mechanisms as a nexus for therapeutic exploitation (Cowan and Ciulli, 2022; Jevti et al., 2021). Despite growing lists of ubiquitin targets, a lack of knowledge regarding how substrates are recognized continues to impede progress and creates a situation in which a vanishingly small number of E3s have their bona fide substrates identified and verified (Iconomou and Saunders, 2016).

E3s are classified according to the mechanism by which they effect Ub transfer to substrate and by the types of domains used to carry out the transfer. RING-Between-RING (RBR) E3s share a three-domain catalytic module consisting of an E2-binding RING1 domain and a catalytic cysteine-containing Rcat (also known as RING2) that are separated by a

zinc-coordinating in-between-RING (IBR) domain. Additional idiosyncratic regions play roles in auto-inhibition and in protein-protein interactions (Cotton and Lechtenberg, 2020; Dove and Klevit, 2017). Although the targets of RBR E3s regulate critical processes, including mitophagy, inflammation, and development, substrate binding domains have yet to be identified for any of the 14 human RBRs (Aguilera et al., 2000; Eiyama and Okamoto, 2015; Elmehdawi et al., 2013; Haas et al., 2009; Iwai et al., 2014; Pickrell and Youle, 2015; Qiu and Fay, 2006; Tan et al., 2018, 2003).

HHARI is an essential RBR with roles in genotoxic stress signaling and organogenesis (Dove et al., 2017a; Hart et al., 2015; Poush et al., 2018; von Stechow et al., 2015; Wang et al., 2015). Several substrates have been identified as targets for HHARI-mediated mono-ubiquitination, yet despite the overt requirement of an E3-substrate interaction, substrate recognition domains have remained elusive (Dove et al., 2017a; Gradilla et al., 2011; Scott et al., 2016; Tan et al., 2018; von Stechow et al., 2015). HHARI is a member of a subset of RBRs that are auto-inhibited by a C-terminal Ariadne domain that occludes the Rcat active site cysteine (Duda et al., 2013). Ubiquitin transfer by RBRs requires formation of an Rcat~Ub intermediate (Wenzel et al., 2011), implying that Rcat must be released from the Ariadne domain to expose the active site Cys for substrate ligation. While substrates must ultimately interact with an activated RBR, how E3 domain rearrangements affect the temporal accessibility of substrate recognition domains remains unclear.

Recent studies identified HHARI as a catalytic component of Cullin-RING ligase (CRL) complexes, in which HHARI can be activated through direct interactions with Neddylated Cul 1, 2, 3, or 4B (Dove et al., 2017a; Horn-Ghetko et al., 2021; Kelsall et al., 2013; Scott et al., 2016). This association promotes HHARI-mediated mono-ubiquitylation of CRL-bound substrates, which are subsequently poly-ubiquitylated by a CRL-bound E2. Thus CRL complexes poise the HHARI Rcat domain for CRL substrate priming (addition of the first Ub) without requiring HHARI to directly recruit a substrate. The *Drosophila* homolog of HHARI, Ariadne-1, interacts with and mono-ubiquitinates substrates *in vitro* in the absence of Cullin components, suggesting HHARI has CRL-independent substrates and, possibly, CRL-independent modes of activation (Gradilla et al., 2011; Tan et al., 2018).

To investigate the determinants for substrate-level mono-ubiquitylation by HHARI in the absence of CRLs, we studied its activity and interaction with the substrate, mammalian translational repressor, 4EHP. Following genotoxic stress, 4EHP is mono-ubiquitylated at detectable levels and its association with the mRNA 5' cap is dependent on HHARI, although its modification by HHARI has not been shown directly (von Stechow et al., 2015). Here we use an integrated structural approach that combines cross-linking mass spectrometry (XL-MS), nuclear magnetic resonance (NMR) spectroscopy, and hydrogen-deuterium exchange mass spectrometry (HDX-MS) to investigate an alternative activation mechanism for HHARI. We demonstrate that mimicry of a phosphorylation event observed in cells activates HHARI robustly. We also characterize 4EHP as a bona-fide HHARI substrate that requires neither a CRL nor its associated E2 and map the E3-substrate interaction to a distinct surface on the HHARI catalytic Rcat domain. Together, these data define a direct substrate binding site for an RBR E3 ligase suggesting a general model for how RBR E3s recognize substrates.

## RESULTS

### An Ariadne domain phosphomimetic mutation activates HHARI

Cellular modes for CRL-independent HHARI activation have yet to be identified. However, phosphorylation modulates the activity of some RBRs, including Parkin and RNF216 (Aguirre et al., 2018, 2017; Condos et al., 2018; Cotton et al., 2021; Kumar et al., 2015; Ordureau et al., 2015; Sauvé et al., 2018, 2015; Seenivasan et al., 2019). Two sites of phosphorylation in HHARI, S427 and S517, were previously identified in a high throughput phospho-proteomic analysis of human ovarian and xenograft breast tumors (Figure 1A–B) (Mertins et al., 2014). Both serine residues are located in the auto-inhibitory Ariadne domain, with S427 located on a helix implicated in activation by CRLs, and that forms the interface with Rcat (Horn-Ghetko et al., 2021).

To test the possibility that a phosphorylation event might lead to activation of HHARI, we introduced aspartic acid mutations to mimic serine phosphorylation at each site and assessed the effects on intrinsic HHARI activity. As previously shown, wild-type HHARI has almost undetectable auto-ubiquitylation activity, while a triple point mutant (F430A, E431A, E503A; HHARI<sup>FEE</sup>) in the Ariadne domain previously shown to overcome auto-inhibition exhibited robust activity (Figure 1C) (Duda et al., 2013; Kellsall et al., 2013). HHARI auto-ubiquitylation was similarly enhanced with HHARI<sup>S427D</sup>, while HHARI<sup>S517D</sup> showed minimal to no change in ubiquitylation levels (Figure 1C). HHARI S427 is adjacent to residues F430 and E431, suggesting that changes at the Ariadne/Rcat interface can lead to activation.

HHARI shares 35% overall sequence identity with the related Ariadne-containing RBR Triad1 (AriH2), and 43% comparing the C-terminal Rcat-Ariadne domains. Of the two observed phospho-sites in HHARI, S427 is conserved as a serine in Triad1, but S517 is not. A phosphomimetic mutation in the analogous Triad1 residue S378 (equivalent position to HHARI S427) also activated Triad1 for auto-ubiquitylation (Figure S1A). Altogether the data establish that S427D HHARI is activated for Ub transfer, at least to itself, and that its mode of activation is shared by another Ariadne RBR, Triad1. The results strongly imply that phosphorylation of HHARI at S427, a modification observed in cells, represents an alternate mechanism for activation to the previously described CRL-dependent mechanism. We therefore chose to use S427D HHARI as the proxy for activated HHARI in our studies.

### HHARI mono-ubiquitylates 4EHP

Given that 4EHP is mono-ubiquitylated at detectable levels and associates with HHARI following genotoxic stress in cells, we sought to evaluate its potential role as a CRL-independent HHARI substrate. To assess whether HHARI associates directly with 4EHP, we examined binding of recombinant, purified 4EHP to auto-inhibited- and active HHARI<sup>S427D</sup> by comigration over gel filtration chromatography (Figure S1B). 4EHP coelutes with both active and auto-inhibited E3 states, consistent with formation of a long-lived complex. 4EHP also co-elutes with the E2/E3 HHARI/UbcH7 complex (with iso-peptide-linked UbcH7-Ub, a stable proxy for E2~Ub). Such a ternary complex contains the minimal components for an E3 ubiquitylation reaction (E2-Ub, E3, substrate). Thus, although not *required*

mechanistically, the results show that the RBR E3 can bind E2~Ub and a putative substrate simultaneously.

While auto-inhibited HHARI binds its E2~Ub with high affinity, this binding does not release inhibition (Dove et al., 2017b; Yuan et al., 2017). How substrate binding might affect RBR activity is not known. To assess whether substrate binding is sufficient to release HHARI auto-inhibition, we reconstituted a 4EHP ubiquitylation reaction *in vitro*. 4EHP was not modified by wildtype HHARI, indicating that neither E2~Ub nor substrate (or both) are sufficient to activate HHARI. In contrast, 4EHP was ubiquitylated primarily with a single ubiquitin in the presence of either active HHARI species (S427D and FEE) (Figure 1C). Reactions performed with a lysine-less ubiquitin (K0), which does not form lysine-linked chains, did not alter the ubiquitylation pattern of 4EHP, confirming that the higher molecular weight bands represent multiple mono-ubiquitylation events (Figure S1C). 4EHP was also mono-ubiquitylated by Triad1<sup>S378D</sup>, suggesting the two related E3s share a conserved substrate-binding surface (Figure S1A). The ability of HHARI<sup>S427D</sup> to robustly ubiquitylate 4EHP in the presence of E1, E2, and Ub, but the absence of a CRL confirms that 1) 4EHP is a CRL-independent HHARI substrate and 2) such substrates bind directly to HHARI, in contrast to CRL-dependent substrates which bind to a CRL subunit.

### XL-MS reveals Rcat mobility

The formation of an E3~Ub intermediate requires Ub transfer between domains that are > 50 Å apart in auto-inhibited HHARI structures. Our data demonstrate that phosphorylation of HHARI is sufficient to stimulate active HHARI conformations in the absence of CRL scaffolds. While 4EHP binding does not increase HHARI reactivity, its presence in a stable auto-inhibited complex may place additional restraints on active HHARI domain architecture. To determine domain rearrangements and interdomain contacts due to phosphomimetic activation and to direct substrate binding, we performed cross-linking mass spectrometry of HHARI in the presence or absence of 4EHP. This approach relies on the physical proximity of residues, providing information on the dynamics and topology of cross-linked regions.

Extensive inter- and intramolecular HHARI and 4EHP cross-links were observed upon incubation with the amine-reactive cross-linker disuccinimidyl suberate (DSS) (Merkley et al., 2014). Several cross-links exceeded the distances expected for DSS cross-linking range ( 30 Å Cα-Cα), with a subset formed between distant N- and C-terminal domains in auto-inhibited samples (Figure 2A–B). The detection of such cross-links involving Rcat residue K346 and the UbaL domain in auto-inhibited HHARI implies that active conformations may be visited without an ‘activating event’, albeit at low frequency. Such low frequency events may account for the basal activity seen in auto-inhibited activity assays. Indeed, when mapped onto a CRL-activated HHARI structure the observed cross-link distances fall within the expected range (Figure 2A–B). We hypothesized that activation promotes an increase in active state conformational sampling and/or maintains HHARI in a reactive state. To test this, we performed a quantitative analysis of select HHARI-HHARI and HHARI-4EHP cross-links (Figure 2C, Figure S2A). Of these, 6/11 intra-HHARI cross-links were consistent with distances observed in both the auto-inhibited and CRL-activated HHARI atomic

structures. Consistent with activation promoting N- and C-terminal domain proximity, an increase in RING1-Rcat cross-links (K257-K346) are observed in HHARI<sup>S427D</sup> (Figure 2C). Several cross-links were observed between sites > 50 Å apart (K168-K293; K257-K398) in both auto-inhibited and CRL-activated structures. These pairs contain residues within flexible linkers, suggesting our cross-linking reactions may detect conformations not captured by static crystal or CryoEM structures currently available. These results demonstrate that HHARI is dynamic even while auto-inhibited and that activating events, such as phosphorylation, can enhance Rcat-RING1 proximity in the absence of an activating CRL complex.

### Rcat C-terminal residues form a substrate binding platform

Consistent with the long-lived HHARI/4EHP complexes observed by SEC, numerous intermolecular cross-links were observed for both auto-inhibited and phosphomimetic E3 states (Figure S1B). In both cases, these cross-links predominantly localized between 4EHP residue Lys83 and the HHARI Rcat region (Figure 3A). This was a surprising finding, as we had anticipated that substrate specificity would probably arise from a domain that is idiosyncratic to HHARI, rather than one that is shared among all RBRs.

We sought to further define the interaction implied by the preponderance of cross-links observed between 4EHP and Rcat. The Rcat domain retains its native conformation when expressed as an isolated domain and is amenable to solution NMR approaches (Dove et al., 2016; Spratt et al., 2013). NMR titration experiments were carried out on <sup>15</sup>N-Rcat with addition of 4EHP. A majority of Rcat peaks were unaffected by 4EHP, while a subset broadened or disappeared completely (Figure S3A–B). Based on previous resonance assignments for the HHARI Rcat domain, the broadened peaks correspond to residues from the C-terminal end of Rcat: these form a contiguous surface that is adjacent to the Rcat active-site cysteine (Figure 3B) (Spratt et al., 2013). Mapping the 4EHP-affected residues onto structures of HHARI reveals that the surface is accessible for binding in both auto-inhibited and CRL-activated high-resolution HHARI structures (Figure 3C–D). Thus, although the NMR experiments were performed on isolated Rcat domain, the results are congruent with relevant multi-domained structures, providing confidence that the surface mapped is indeed the 4EHP binding site.

Co-purification of a ternary complex of HHARI<sup>S427D</sup>, 4EHP, and UbcH7-Ub implies that 4EHP can bind HHARI during the transthiolation step between the RING1-bound E2~Ub and Rcat. Previously, we identified a Ub binding surface on Rcat that is important for E2-E3 transthiolation, begging the question: can both 4EHP and Ub bind to the small Rcat domain simultaneously (Dove et al., 2016)? To address this, Ub was added to <sup>15</sup>N-Rcat/4EHP complexes and NMR spectra were collected. Perturbations to the previously reported Rcat Ub binding surface are observed, and these are distinct from the 4EHP binding site (Figure S3C–D). The structure of a CRL-activated HHARI/UbcH7-Ub transthiolation complex was recently captured by cryo-EM using a tripartite active site trap (Horn-Ghetko et al., 2021). In this structure, the Ub C-terminus is poised for transfer to the Rcat catalytic cysteine through interactions with the HHARI IBR-Rcat Ub guide helix. From our studies, the Rcat surface perturbed by Ub binding (in the context of an isolated Rcat and 4EHP complex) aligns with

the cross-linked Ub from the CRL-activated state (Figure 3E, Figure S3C–D). Altogether, the results demonstrate that 1) HHARI's Rcat has distinct binding surfaces for its substrate, 4EHP, and the donor Ub and 2) 4EHP that is bound to auto-inhibited HHARI can also remain bound during the first step of Ub transfer, namely the transthiolation, after HHARI becomes activated.

### HDX reveals ternary complex conformational rearrangements

Our understanding of RBR mechanisms has been limited to snapshots of auto-inhibited or activated states for a given RBR E3. The use of multi-functional probes allows the trapping of distinct functional conformers, however gaps in understanding dynamic intermediate states still remain. Hydrogen-deuterium exchange mass spectrometry (HDX-MS) is a powerful approach for studying protein complexes and their dynamics in solution (Engen, 2009). The exchange of protein backbone amide hydrogen atoms with deuterium atoms from  $^2\text{H}_2\text{O}$  is followed as a function of time and read out by mass spectrometry as each deuterium incorporated adds 1 Dalton to the mass. The rate at which exchange occurs depends on local structure and stability: an amide that is involved in hydrogen bonds or that is less accessible to solvent will exchange more slowly than one that is highly flexible and/or exposed to solvent. Thus, the degree of protection from deuteration is indicative of local structure and dynamics. While XL-MS and NMR identified domain rearrangements and 4EHP-Rcat interactions, local changes in structure and conformation associated with S427D activation are not captured. Therefore, we performed HDX-MS on a variety of HHARI complexes to assess the contribution of each protein state on HHARI domain structure. To enable comparison of data between different protein states, every time point was taken in triplicate and statistical significance was determined (see Methods, and Supplementary Table 2 HDXMS Summary, related to Figures 4–6, S4).

The HDX-MS profiles of auto-inhibited and activated HHARI<sup>S427D</sup> were compared to assess changes in the E3 itself. Significant differences in deuterium uptake kinetics were observed for peptides from the HHARI Rcat-Ariadne interface (Figure 4). By far, the largest difference in deuterium uptake was observed for peptides in the Ariadne region surrounding S427: the relevant peptides are strongly protected in auto-inhibited HHARI and exchange much more readily in HHARI<sup>S427D</sup> (Figure 4). This region of the Ariadne domain was recently termed the 'switch-helix' because HHARI binding to Cul1 is associated with an allosteric kinking of Ariadne helical residues that is thought to induce the release of Rcat (Horn-Ghetko et al., 2021). Notably, an exchange boundary is observed in which the C-terminal portion of the switch-helix shows decreased exchange upon phosphomimetic activation, suggesting changes in secondary structure stability. Alignment of auto-inhibited and CRL-activated switch-helices reveal the boundary defined by exchange corresponds to the helical transition pivot point, showing remarkable congruence of the HDX and cryo-EM data (Figure 4). Additionally, peptides located on the Rcat surface that contains the catalytic cysteine, normally occluded by the Ariadne domain by auto-inhibition, showed an increase in deuterium uptake kinetics. No other significant changes in deuterium uptake were observed throughout HHARI, suggesting that the activation for HHARI<sup>S427D</sup> arises from conformational changes in the Ariadne switch helix and concomitant Rcat release.

Thus, while HHARI activation is mediated in at least two ways, via CRL interactions and phosphorylation, the mechanisms that effect Rcat release share common features.

Turning next to changes associated with binary complex formation, HDX profiles of HHARI bound to its preferred E2-Ub conjugate, UbcH7-Ub, were compared to the apo-E3. The differences in deuterium uptake associated with E2-Ub binding were isolated, with a decrease in exchange at the known RING1/UbcH7-Ub binding site (Figure S4A–B) (Dove et al., 2017b). Additionally, helix 1 of the UbaL domain shows increased exchange in the presence of UbcH7-Ub. This helix sits atop a kinked RING1-IBR linker helix that undergoes allosteric straightening upon Nedd8-Cul1 binding (Horn-Ghetko et al., 2021). No significant changes in deuterium uptake are seen in the Rcat or Ariadne domains, consistent with both crystal structures and in vitro auto-ubiquitylation assays which indicate that association of UbcH7-Ub with HHARI does not induce HHARI activation (Dove et al., 2017b; Yuan et al., 2017). Unlike canonical RING domains that keep E2-Ub conjugates in a ‘closed state’ to promote aminolysis reactivity, HHARI RING1 promotes an open conformation for transthiolation (Dove et al., 2017b). Two currently available auto-inhibited HHARI/UbcH7-Ub x-ray structures have provided differing views of the location of the Ub moiety (Dove et al., 2017b; Yuan et al., 2017). One structure has weak density for the Ub, consistent with it being either dynamic or heterogeneous (Dove et al., 2017b). In the other structure, the Ub is associated with the UbaL domain of HHARI (Yuan et al., 2017). Our HDX results show no additional protection consistent with a long-lived association of Ub with the UbaL. Ub interactions with the Rcat-IBR linker (Ub guide helix), however, are required for transthiolation (Dove et al., 2016; Horn-Ghetko et al., 2021). A cryo-EM structure of the CRL-HHARI/UbcH7-Ub complex was made possible by covalently trapping the transthiolation species using a tripartite crosslinker. No significant change in deuterium uptake was seen for peptides associated with this intermediate, although we were able to detect Rcat/Ub interactions via NMR (Figure S3C–D). This suggests the Rcat/E2-Ub interaction captured in the tripartite trap is transient in solution.

HDX-MS data provides insight into possible allosteric effects induced by complex formation (Peacock and Komives, 2021; Ramirez-Sarmiento and Komives, 2018). To assess changes in E3 and substrate upon binding, complexes of 4EHP bound to auto-inhibited and HHARI<sup>S427D</sup>, in the absence of UbcH7-Ub, were compared. The presence of 4EHP led to a single region of HDX protection in the Rcat and Ariadne domains of both auto-inhibited and HHARI<sup>S427D</sup> complexes (Figure 5A–C). Rcat C-terminal peptides exhibited a decrease in deuterium uptake kinetics, as did the Rcat-Ariadne linker and the distal start of the Ariadne switch helix (Figure 5C). This region of the switch helix shows variable density in current high-resolution structures, with secondary structure starting between residues R401-A410. These observed effects are consistent with both the XL-MS and NMR mapping. Additionally, HHARI<sup>S427D</sup> complexes showed enhanced protection adjacent to the switch helix, at the hinge region of Ariadne helices 2 and 3 at early timepoints (Figure 5C). Given the high affinity association of 4EHP with Rcat in the absence of the Ariadne domain, it remains unclear whether the decrease in deuterium on the Ariadne domain is due to stabilization of the terminal switch helix residues, or to direct binding of 4EHP. Increased protection was also observed within Rcat Ub guide helix and catalytic cysteine-containing peptides in the 4EHP/HHARI<sup>S427D</sup> complex (Figure 5B). The Ub guide helix exists as an

unstructured IBR-Rcat linker in the auto-inhibited HHARI state, but forms helical secondary structure that positions Ub during transthiolation upon activation (Duda et al., 2013; Horn-Ghetko et al., 2021). Helical formation is also detected in solution structures of isolated Rcat, which were used in this study as a proxy for the activated state of HHARI (Spratt et al., 2013). Our NMR results showed no significant perturbations to Ub guide helix resonances upon addition of 4EHP, suggesting the changes in activated E3 HDX are due to allostery rather than direct interactions with 4EHP.

Comparison of ternary complexes composed of HHARI, 4EHP, and UbcH7-Ub with each of the binary complexes revealed no additional differences in HDX. This suggests the driving force of activation is release of Rcat brought about by a conformational change in the Ariadne switch helix. Furthermore, no significant changes in either UbcH7 (other than RING1 binding) or Ub were observed in the ternary complexes. Although the HHARI<sup>S427D</sup>/4EHP/UbcH7-Ub complex represents a fully primed transthiolation complex, requiring Rcat and the E2-Ub catalytic sites to come into proximity for catalysis, these interactions are likely short lived and do not result in detectable changes in HDX kinetics within the time scale of our experiments (shortest time point of 3 s).

Finally, a distinct surface on 4EHP was protected in both binary and ternary complexes (Figure 6A–C). The results provide further confirmation that 4EHP binds to HHARI in a highly similar manner, whether HHARI is auto-inhibited, activated, or primed for catalysis with its E2~Ub. The peptides that showed decreased deuterium uptake are located on a surface that surrounds W95 and is opposite from the mRNA cap binding pocket of 4EHP. In translation repression complexes, 4EHP interacts with proteins using a similar W95-centered surface, suggesting HHARI and mRNA cap binding need not be mutually exclusive (Peter et al., 2017).

### Model of HHARI-4EHP complexes

To create a structural model for HHARI-substrate interactions, we combined our solution-based insights with published crystallographic and cryo-EM structures. In separate runs, restraints from the Rcat-4EHP NMR studies, with or without additional XL-MS restraints, were input into the HADDOCK docking program along with the 4EHP structure (PDB: 2JGC) and auto-inhibited HHARI (PDB: 4KC9) (Honorato et al., 2021; van Zundert et al., 2016). The resulting models converge on a complex that positions 4EHP helix 1 and 2 with the C-terminal surface of Rcat, leaving the 4EHP mRNA cap binding pocket solvent accessible (Figure 7A). Haddock Cluster 4, with the second highest Haddock score from runs that included XL-restraints, was selected as the top model, given that the orientation of 4EHP relative to the Rcat-Ariadne domains is consistent with the pattern of decreased deuterium uptake in HHARI-4EHP complexes (Figure S5A, Supplementary Table 1). Additionally, the highest scoring Haddock Cluster from runs without XL-MS restraints modeled 4EHP in a similar orientation (Figure S5B). Alignment of the Cluster 4 Rcat domain with activated Rcat (PDB: 7B5L) positions 4EHP in a cavity bounded by the Ariadne domain and Rcat/UbaL domains during transthiolation (Figure 7B). Mutation of HHARI Rcat residues within the modeled interface revealed W386 and Y387 as important residues for Rcat-4EHP interaction, with disruption of this surface resulting in

loss of complex formation on size-exclusion chromatography (Figure 8A–D). While W386A dramatically reduced 4EHP ubiquitylation, HHARI Y387A maintained the ability to mono-ubiquitylate 4EHP at near wildtype levels (Figure 8A–B). The identification of Rcat mutants that weaken binding but are still able to ubiquitylate 4EHP is consistent with transient E3:substrate interactions, and suggests that high affinity substrate interactions are not required for HHARI-mediated ubiquitin transfer. Reciprocal attempts to identify individual 4EHP residues with similarly strong effects were unsuccessful. A common feature of 4EHP complex assemblies is recognition of the 4EHP dorsal surface, including hydrophobic interactions with W95, however, 4EHP W95A did not disrupt HHARI association or ubiquitylation under the conditions tested (data not shown). In addition to dorsal surface interactions, a subset of 4EHP-associated proteins interact via noncanonical motifs that increase their affinity to 4EHP (Peter et al., 2017). Intriguingly, a similar noncanonical surface was protected in 4EHP-HHARI HDX-MS complexes, however, a 4EHP mutational scan proved inconclusive due to poor protein solubility. Our data support a model in which positioning of 4EHP relative to auto-inhibited Rcat is still satisfied by tertiary restraints defined by domain placement in activated transthiolation complexes (Figure 7C). Based on current structural data, it is not clear which 4EHP lysine residues are accessible for ubiquitin ligation. Additional conformational rearrangements of Rcat may be needed to fulfill the final substrate ubiquitin ligation step.

## DISCUSSION

The identification of RBR catalytic sites a decade ago ignited efforts to understand their unique mechanistic strategies (Wenzel et al., 2011). While seminal works have identified common themes in RBR transthiolation reactions, two major aspects remain ill-defined. First, it is clear that the mechanisms by which RBRs are released from auto-inhibition differ among family members, so each must be defined individually (Aguirre et al., 2017; Dove et al., 2017a; Duda et al., 2013; Gladkova et al., 2018; Horn-Ghetko et al., 2021; Kelsall et al., 2013; Lechtenberg et al., 2016; Liu et al., 2017; Riley et al., 2013; Sauvé et al., 2018; Stieglitz et al., 2013; Trempe et al., 2013). Second, no substrate binding domains have been identified for any of the RBR E3s. Here we identify a site-specific activation mechanism for HHARI and map a substrate-binding domain for RBR E3s using HHARI and 4EHP as an exemplary pair.

An Ariadne domain substitution (S427D) that mimics a phosphorylation event observed in cells releases HHARI auto-inhibition and promotes both HHARI transthiolation and substrate ligation *in vitro*. Notably, S427 is conserved in the related RBR E3, Triad1, suggesting the possibility that the mechanism of activation by phosphorylation is conserved as well. S427 is in the interdomain interface between the Ariadne and Rcat domains. The presence of negative charge in the form of either the phosphomimic, aspartate, or a bona fide phosphoryl group is sufficient to disrupt the interface and enable release of Rcat and its otherwise sequestered active site. S427 itself is also occluded in the auto-inhibited conformation, raising the question of how its phosphorylation is achieved. Our quantitative XL-MS results indicate that Rcat is released even in auto-inhibited HHARI, albeit at low frequency. It is possible that a kinase can access and modify S427 during such an event and, once modified, the Ariadne domain will remain disengaged from Rcat. An

alternative possibility is that S427 may be phosphorylated while HHARI is bound to a CRL, as the serine is accessible in this conformation. We propose that either mechanism is possible and further investigations will be needed to define the phosphorylation mechanism. Regardless of how phosphorylation is carried out, the RBR E3s shown to be activated by phosphorylation now include Parkin (known previously), HHARI, and Triad1 (this study).

The mechanism revealed for activation by phosphorylation of HHARI has parallels with that recently shown for CRL-activation of HHARI, in which direct interactions between Neddylated-Cul1 and HHARI Ariadne and UbaL domains lead to the allosteric release of Rcat (Horn-Ghetko et al., 2021). Importantly, the phosphomimetic model presented here and the CRL-activated mechanism both involve allosteric changes in Ariadne helix 1, termed the switch helix, although the outcome is achieved in different ways. We therefore propose that disruption of the Rcat-Ariadne interface is a common mechanism for HHARI activation and that this can be achieved in at least two ways: allosterically through a direct protein-protein interaction or by direct phosphorylation of HHARI. There are also important differences in the mode of action of HHARI in CRL-dependent versus CRL-independent reactions. Although in both cases, HHARI is responsible for placing a single Ub on a target protein, HHARI's Rcat mediates ligation to CRL-bound substrates in the former case and to HHARI-bound substrates in the latter. Whether the substrate-binding site defined by our study plays a role during Ub transfer to a CRL-bound substrate remains to be determined.

While many E3-substrate interactions are transient, 4EHP forms a high affinity complex with HHARI in both inhibited and activated conformations. The finding suggests a model wherein upon activation, substrate-bound Rcat is released from its Ariadne binding site and traverses the length of HHARI to the RING1-bound E2~Ub. The long-range journey is made possible by the long, flexible linkers that connect Rcat to its neighboring domains. As shown in Figure 7C, we envision this process akin to a trapeze (Rcat) and its artist (substrate) swinging from one side of HHARI to another.

Our study identified a di-aromatic motif within Rcat as critical for substrate binding to HHARI. A non-overlapping set of Rcat residues are involved in binding Ub and form a surface for donor-Ub orientation during transthiolation (Dove et al., 2016; Horn-Ghetko et al., 2021). Our results demonstrate that the two binding sites can be occupied simultaneously, suggesting that 4EHP is poised for Ub ligation transfer. Notably, the C-terminal region of Rcat has been implicated in Ub chain formation for RBR's such as HOIP and RNF216 (Cotton et al., 2021; Stieglitz et al., 2013). These RBRs contain a zinc finger insert (ZF1) that positions an acceptor ubiquitin lysine (the substrate in a chain-building reaction) for ligation to the Rcat-linked donor Ub C-terminus. Sequence alignment reveals that these inserts, while unique to HOIP and RNF216, are located within the region of Rcat that is protected by 4EHP binding, and adjacent to the Rcat catalytic cysteine (Figure 9A). We propose that substrate binding, whether ubiquitin or non-ubiquitin in nature, may be a general feature for C-terminal Rcat residues, and that sequence divergence in this region may determine substrate specificity.

Intriguingly, virtually all human RBR E3s contain di-aromatic motifs within their Rcat domains. Triad1, ANKIB1, and CUL-9 contain di-aromatics in analogous positions to

HHARI, within the loop between the final two Zn ligands of Rcat (Figure 9A–B). In each case, the surrounding residues are not conserved implying that the aromatic landing pad is in a unique environment in each E3, perhaps providing substrate specificity. On this basis, we posit that these four RBRs directly bind and modify their substrates and are likely not poly-Ub chain building E3s.

Four E3s, parkin, Dorfin, RNF19B, and Triad2 have di-aromatics that are either observed experimentally or are predicted by AlphaFold to reside near the active site Cys residue and occlude it. In these cases, the aromatics are just past the final Zn ligand (Figure 9A–B). In parkin, the WY motif is in the interface between Rcat and R0 and will only become accessible after release of Rcat in activated parkin.

The large domain rearrangements and the dynamic behavior that appear to characterize the strongly auto-inhibited RBR E3 family pose challenges to understanding their mechanisms in detail. Here, we illustrate how an integrated structural approach can provide new insights regarding the conformational gymnastics of HHARI, a strategy that is proving impactful for the study of dynamic E3s (Faull et al., 2019). Our work expands understanding of both E3 activation and substrate interactions. Somewhat unexpectedly, the identified substrate-binding domain, i.e., Rcat, is one of the shared domains within the RBR module rather than a unique domain. We propose that sequence divergence in the relevant region of Rcat domains supports substrate selection among RBR E3s. Manipulation of this region will enable evaluation of other RBRs and could facilitate substrate identification—the remaining aspect of RBR function to be conquered.

## STAR METHODS

### RESOURCE AVAILABILITY

**Lead contact**—Further information and requests for resources and reagents should be directed to and will be fulfilled by the Lead Contact, Rachel E. Klevit (klevit@uw.edu).

**Materials availability**—Plasmids generated in this study are available by request from the Lead Contact, Rachel E. Klevit (klevit@uw.edu).

### Data and code availability

- All raw and processed XL-MS data discussed in this paper are available via the ProXL web application at: <https://proxl.yeastrc.org/proxl/p/hhari> (Riffle et al., 2019, 2016). In addition, complete search algorithm configuration files, FASTA search databases, raw search output and raw MS data files were deposited to the ProteomeXchange Consortium via the PRIDE partner repository with the dataset identifier PXD030849 (Vizcaíno et al., 2009). Full Skyline quantification data of all XL-MS experiments were deposited to the ProteomeXchange Consortium via Panorama Public and is available at: <https://panoramaweb.org/hhari.url> with the dataset identifier PXD030871 (Sharma et al., 2018). Data can also be requested directly from the corresponding author.
- This paper does not report original code.

- Any additional information required to reanalyze the data reported in this paper is available from the lead contact upon request.

## EXPERIMENTAL MODEL AND SUBJECT DETAILS

All purified proteins used in biochemical, biophysical, and structural experiments were recombinantly expressed in *E. Coli* (see below). All genes are of human origin.

## METHOD DETAILS

**DNA manipulation and protein purification**—The following constructs were used in this study, and if not stated otherwise, are human and full-length: HHARI<sup>WT</sup>, HHARI<sup>F430A/E431A/E503A</sup>, HHARI<sup>S427D</sup>, or HHARI<sup>S517D</sup>, HHARI<sup>N-WT</sup> or HHARI<sup>N-S427D</sup> (aa 90–557), HHARI-Rcat (aa 325–396), Triad1<sup>WT</sup> or Triad1<sup>S378D</sup>, 4EHP (aa 45–225 or 45–234), UbcH7<sup>WT</sup> or UbcH7<sup>C86K</sup>, Uba1, Ub<sup>WT</sup>, Ub<sup>K0</sup> or HA-Ub. HHARI, HHARI-Rcat, and Triad1 were cloned into pGEX-4T2 in-frame with TEV cleavable, N-terminal His<sub>6</sub>-GST tag. HHARI<sup>N</sup> and 4EHP (aa 45–225) were cloned into pGEX-6p1 in-frame with Precision Protease cleavable, N-terminal GST-tag. 4EHP (aa 45–234) was cloned into pET28a in-frame with His<sub>6</sub>-T7 at the N-terminus. Point mutations were introduced using standard Stratagene QuikChange protocols.

Proteins were expressed in LB or minimal MOPS media supplemented with [<sup>15</sup>N]-ammonium chloride in *Escherichia Coli* (BL21 DE3 cells) until optical density reached a value of 0.6, at which point cells were induced with 200 μM IPTG and grown at 16°C for 18 hours unless otherwise stated. Media for E3s was supplemented with 0.2 mM ZnCl<sub>2</sub>. Human His<sub>6</sub>-Uba1 was purified as follows. Premade ubiquitin-conjugated resin was equilibrated with 50 mM Tris HCl pH 8.0. A final concentration of 40 mM ATP pH 7.0, 40 mM MgCl<sub>2</sub> was added to clarified *E. Coli* lysate, and the mixture was incubated with the ubiquitin resin for 1 hour at room temperature. The column was washed with 50 mM Tris pH 8.0, 0.5 M KCl until the flow through 260 nm absorbance reading was near zero. E1 was eluted with 50 mM Tris pH 8.0, 10 mM DTT and pooled elutions were dialyzed into 25 mM sodium phosphate pH 7.0, 150 mM NaCl, 1 mM DTT overnight at 4°C. Dialyzed sample was concentrated to 40 μM with the addition of 5% glycerol for storage. GST-HHARI and GST-Triad1 were purified using glutathione Sepharose 4B resin (GE healthcare) in 25 mM Tris, 150 mM NaCl, 1 mM DTT, pH 7.5, and eluted with 20 mM glutathione. GST-tags were cleaved with TEV protease during overnight dialysis in 25 mM Tris, 150 mM NaCl, 1 mM DTT, pH 7.5 at 4°C and removed by anion-exchange chromatography (25 mM Tris, 0–1 M NaCl gradient, 1 mM DTT, pH 7.5). GST-HHARI<sup>N</sup> was purified using glutathione Sepharose resin in 25 mM Tris, 150 mM NaCl, 1 mM DTT, pH 8.5. GST-tags were cleaved on column with Precision protease and removed by size-exclusion chromatography (25 mM Tris, 150 mM NaCl, 1 mM DTT, pH 7.5). GST-4EHP (aa 45–225) was purified using glutathione Sepharose resin in 20 mM HEPES, 150 mM NaCl, 1 mM DTT, pH 7.5. GST-tags were cleaved on column with Precision protease and removed by cation-exchange chromatography (20 mM HEPES, 0–1 M NaCl, 1 mM DTT, pH 7.5) and size-exclusion chromatography (25 mM Tris, 150 mM NaCl, 1 mM DTT, pH 7.5). His<sub>6</sub>-T7 4EHP (aa 45–234) was purified using Ni<sup>2+</sup> affinity chromatography. His-tags were cleaved with thrombin and dialyzed into 20 mM HEPES, 50 mM NaCl, 2 mM DTT, pH

7.5. Thrombin was captured with p-Aminobenzamidine-Agarose (Sigma) and His-tags were separated by cation-exchange chromatography (20 mM HEPES, 0–1 M NaCl, 1 mM DTT, pH 7.5).

HHARI-Rcat used for NMR was inserted into pGEX-4T2H modified with a TEV cleavage site. The plasmid was transformed into *E. Coli* BL21 DE3 competent cells and cells were <sup>15</sup>N-labeled and expressed using a high density minimal media prep adapted from (Marley et al., 2001). Cells were initially grown in LB at 37°C until OD<sub>600</sub> = ~0.6, at which point cells were harvested by centrifugation at 4000 rpm for 12 minutes at 4°C. Cell pellets were resuspended in 40 mM MOPS-KOH pH 7.0, 4.5 mM Tricine, 50 mM NaCl, 1g/L NH<sub>4</sub>Cl at 4°C. Combined resuspensions were centrifuged at 4000 rpm for 12 minutes at 4°C. Cell pellets were resuspended in 1/10 final culture volume with MOPS complete media supplemented with 1g/L 99% [<sup>15</sup>N]-ammonium chloride, 100 µg/mL ampicillin, and 0.2 mM ZnCl<sub>2</sub>. Cultures were distributed to baffled Fernbach flasks containing complete MOPS media, with a ratio of 1L MOPS media to 4L initial LB growth. Resuspended cultures were grown at 16°C for 1 hour prior to induction with 200 µM IPTG for 18–20 hours. Cells were harvested at 4000 rpm at 4°C and lysed in 20 mM Tris pH 7.4, 120 mM NaCl, 5 mM DTT, supplemented with 1 mM PMSF, cOmplete EDTA-free protease inhibitors (Sigma), DNase, RNase, and lysozyme. Lysis was performed by French press followed by clarification at 16000 rpm for 25 minutes at 4°C. The supernatant containing GST-Rcat was applied to a gravity column containing Glutathione Sepharose 4B resin and washed with 5 column volumes of 20 mM Tris pH 7.4, 120 mM NaCl, 5 mM DTT. GST-Rcat was eluted with 20 mM glutathione and cleaved with TEV protease overnight at 4°C with dialysis into 25 mM Tris pH 7.5, 100 mM NaCl, 1 mM DTT. Cleaved Rcat was separated on a monoQ column over a gradient of 0–500 mM NaCl in Tris pH 7.5, 1 mM DTT. Rcat was concentrated and applied to a size exclusion column (Superdex 75) equilibrated in 25 mM MES pH 6.5, 150 mM NaCl, 5 mM DTT. Pure samples were concentrated, flash frozen, and stored at –80°C.

UbcH7 (WT and C86K) cell pellets were resuspended in 25 mM NaPi pH 7.6, 50 mM NaCl, supplemented with 1 mM DTT, 1 mM PMSF, cOmplete EDTA-free protease inhibitors (Sigma), DNase, RNase, and lysozyme. Lysis was performed by French press followed by clarification at 16000 rpm for 25 minutes at 4°C. The supernatant containing soluble E2 was passed through a 0.45 µm filter prior to application to HiTrap SP (Cytiva). UbcH7 was eluted over a gradient of 0–200 mM NaCl in 25 mM NaPi pH 7.6. Samples were concentrated and applied to a size exclusion column (Superdex 75) equilibrated in 25 mM NaPi pH 7.6, 150 mM NaCl, 1 mM DTT. Ub was purified as follows. Clarified lysate was transferred to a beaker on ice. While stirring over a period of 2–3 minutes, 70% perchloric acid was added until the pH dropped to 4.5. Lysate was stirred on ice for an additional 30 minutes. The suspension was centrifuged at 17,000 rpm for 25 minutes in an SS34 rotor at 4°C. Supernatant was dialyzed against 50 mM sodium acetate, pH 4.5 (pH adjusted with glacial acetic acid) overnight at 4°C. The following day, additional precipitant was centrifuged at 17,000 rpm for 25 minutes in an SS34 rotor at 4°C. The supernatant was dialyzed in fresh 50 mM sodium acetate, pH 4.5 for an additional 3 hours at 4°C. Dialyzed sample was applied to HiTrap SP (Cytiva) equilibrated in 50 mM sodium acetate pH 4.5, and eluted over a gradient of 0–1 M NaCl. Pure fractions were combined and applied to a

size exclusion column (Superdex 75) equilibrated in 25 mM sodium phosphate pH 7.0, 150 mM NaCl.

**Nuclear magnetic resonance spectroscopy**—Purified,  $^{15}\text{N}$ -labeled HHARI Rcat was concentrated to  $\sim 400\ \mu\text{M}$  using 3-kDa centrifugal ultrafilters (Millipore). 4EHP samples were buffer exchanged using PD midiTrap G-25 columns (GE Healthcare) in 20 mM MES pH 6.5, 150 mM NaCl, 5 mM DTT. All NMR experiments were performed in 10%  $\text{D}_2\text{O}$  on either a Bruker Avance 500-MHz spectrometer or on a Bruker Avance 600-MHz spectrometer fitted with a TCI CryoProbe (Bruker) set to 298K. To characterize the 4EHP binding interface,  $^{15}\text{N}$ -HSQC-TROSY spectra of Rcat ( $150\ \mu\text{M}$ ) were acquired at 4 concentrations of 4EHP ranging from  $0\ \mu\text{M}$  to  $300\ \mu\text{M}$ .

**Generation of non-dischargeable E2-Ub complex**— $5\ \mu\text{M}$  human E1 (Uba1),  $400\ \mu\text{M}$  Ub and  $200\ \mu\text{M}$  UbcH7 $^{\text{C86K}}$  were incubated in 25 mM CAPS, 150 mM NaCl, pH 9.7 at  $37^\circ\text{C}$  with 5 mM ATP, 10 mM  $\text{MgCl}_2$  overnight. Isopeptide linked UbcH7 $^{\text{C86K}}$ -Ub was subsequently purified by size-exclusion chromatography in 25 mM Tris pH 8.5, 200 mM NaCl, 10 mM DTT.

**Hydrogen-deuterium exchange**—HHARI $^{\text{N}}$  and HHARI $^{\text{N-S427D}}$  complexes were incubated with 2X molar excess 4EHP, and or UbcH7-Ub and purified by size-exclusion chromatography (25 mM Tris, 150 mM NaCl, 1 mM DTT, pH 7.5) to isolate 1:1 complexes. PPPI and PPPF (Pro-Pro-Pro-Ile/Phe) tetrapeptides were added to protein stocks as internal exchange standards. Hydrogen-deuterium exchange was initiated by diluting  $10\ \mu\text{L}$  of each complex into  $90\ \mu\text{L}$  deuterated buffer: 25 mM Tris, 150 mM NaCl, 1 mM DTT, pH 7.5, 85%  $\text{D}_2\text{O}$  (Cambridge Isotope Labs), containing  $0.5\ \mu\text{g/mL}$  Angiotensin II, for a final protein concentration of  $100\ \mu\text{g/mL}$ . HDX reactions were conducted in triplicate at room temperature ( $25^\circ\text{C}$ ) and exchange reactions were quenched at 3 s, 60 s, 30 min, 20 hours, with equal volumes of ice-cold quench buffer (8M urea, 0.2% formic acid (FA), 0.2% trifluoroacetic acid (TFA), final pH 2.5), and immediately frozen in liquid nitrogen. Fully deuterated samples of individual proteins were prepared by denaturing samples at  $80^\circ\text{C}$  in 20 mM DTT, 3.5 M guanidine HCl for 30 minutes, diluting in deuteration buffer, and incubating at  $60^\circ\text{C}$  prior to quenching as described above. Undeuterated samples were prepared identically to deuterated samples with water in place of  $\text{D}_2\text{O}$ . A ‘zero’ second control was prepared by premixing the deuteration and quench buffers on ice, prior to the addition of protein and immediately freezing in liquid nitrogen. All HDX buffers were prepared with liquid chromatography-MS (LC-MS) grade Optima Water (Thermo Fisher Scientific).

**HDX Mass-spectrometry**—An in-house automated HDX system was used to improve consistency among runs. Samples were maintained at  $-60^\circ\text{C}$  in a dry-ice and ethanol bath. A PAL LEAP Robot was modified to perform 4 min automated sample thawing and injection (Watson et al., 2021). Samples were digested online with immobilized pepsin for 0.5 min and trapped on a Waters ACQUITY UPLC CSH C18 VanGuard,  $130\ \text{\AA}$ ,  $1.7\ \mu\text{m}$ ,  $2.1\ \text{mm}$  by  $5\ \text{mm}$  trap column for 3 min with a flow of solvent A (2% acetonitrile, 0.1% FA, and 0.025% trifluoroacetic acid) at a rate of  $150\ \mu\text{L/min}$ . Peptides were resolved over

a Waters ACQUITY UPLC CSH C18, 130 Å, 1.7 µm, 1 mm by 100 mm column using a 10-min linear gradient of 3 to 50% solvent B (solvent B: 100% acetonitrile and 0.1% FA) and analyzed using a Waters Synapt G2-Si Q-TOF with ion mobility enabled. The injection loop, lines and columns were kept at 0 °C to minimize back exchange. A series of pepsin column and trap column wash steps were implemented between each injection to minimize carryover (to <5%)(Watson et al., 2021). Undeuterated peptides of each complex component were identified by exact mass and MS/MS spectra on a Thermo Orbitrap and analyzed using Protein Prospector (UCSF). Spectra were analyzed by MassLynx software (Waters Corp), DriftScope (Waters Corp), and HDExaminer (Sierra Analytics). Statistical significance determined by a Welch's Student T-test, as described in (Hageman and Weis, 2019), and data visualization were performed with an in-house HDX analysis R-Suite, HDXBoXer. All peptides described as significant in the text or shown in figures have a significance cut-off of  $p < 0.01$ . To allow access to the HDX data of this study, the HDX data table (Supplementary Table 2 HDXMS Summary, related to Figures 4–6, S4) are included in the supporting information as per consensus guidelines (Masson et al., 2019).

**Model of HHARI-4EHP complex**—Structural modeling of HHARI-4EHP complexes was performed using the web server Haddock 2.4(Honorato et al., 2021; van Zundert et al., 2016). Auto-inhibited HHARI (PDB: 4KC9) and 4EHP (PDB: 2JGC) were used to generate input structures. For the docking, Rcat residues that exhibited significant intensity loss upon 4EHP binding (res 382–390) and 4EHP residues in peptides that showed a decrease in deuterium uptake upon HHARI complex formation (res 89–97) were defined as active residues. Unambiguous restraints were used between 4EHP (K83) and HHARI (K326, K346) with a 30 Å distance limit. Cluster solutions were cross-evaluated for consistency between NMR, HDX-MS, and XL-MS results. Haddock results scores are included in Supplementary Table 1.

**HHARI activity assays**—For E3 auto-ubiquitylation assays, 1 µM human E1, 5 µM UbcH7, 2 µM E3 (HHARI, Triad1) and 20 µM HA-Ub were incubated at 37 °C in 25 mM HEPES, 100 mM NaCl, 0.5 mM DTT, pH 7.5. Reactions were initiated with 5 mM ATP, 10 mM MgCl<sub>2</sub> and quenched with SDS-PAGE reducing buffer. Substrate ubiquitylation assays were performed similarly to auto-ubiquitination, with the addition of 5 µM T7–4EHP. Samples were run on SDS-PAGE gel and visualized on Western blots, blotting for tags on Ub (auto-ubiquitylation) and 4EHP (substrate). Antibodies used were as follows: HA antibody - Bethyl, A190–108A; T7 antibody – Novagen, 69522; Anti-Rabbit DyLight 800, Cell Signaling 5151S; and Anti-Mouse Alexa Fluor 680, Invitrogen, A21058.

### **Chemical Cross-linking and Mass Spectrometry Analysis (XL-MS)**

**Sample preparation:** Chemical cross-linking and mass spectrometry analysis (XL-MS) was carried out as described below. These methods are an adaptation of those described in (Zelter et al., 2015). Reactions were 50 µL total volume in 20 mM HEPES pH 7.5, 100 mM NaCl, 1 mM DTT plus 0.5 mM DSS (disuccinimidyl suberate, ThermoFisher Scientific, Waltham, MA). HHARI only reactions contained 0.2 µg/µl (3.6 µM) HHARI. HHARI plus 4EHP reactions additionally contained 0.08 µg/µL (3.9 µM) 4EHP. Ska core complex was purified as described by and spiked into all reactions at 0.02 µg/µL (1:10 Ska

complex:HHARI weight to weight ratio) as a normalization control(Helgeson et al., 2018). Cross-linking was carried out for 15 mins at room temperature before quenching by addition of 5  $\mu$ L 1 M  $\text{NH}_4\text{HCO}_3$ . Four separate reaction conditions were performed: (1) Wild-type HHARI; (2) Wild-type HHARI + 4EHP; (3) Activated HHARI; (4) Activated HHARI + 4EHP. Each reaction was performed in triplicate. Reactions were performed in random order to minimize batch effects. After quenching, samples were stored at  $-80^\circ\text{C}$  until processing for mass spectrometry analysis.

Reactions were prepared for MS analysis by bringing them up to 0.1% PPS silent surfactant (Expedion Inc. San Diego, CA), 5 mM TCEP (tris(2-carboxyethyl)phosphine). Samples were reduced for 60 mins at  $60^\circ\text{C}$  in an Eppendorf Thermomixer with shaking (1200 rpm). Alkylation was performed at room temperature in the dark for 20 mins with 6 mM iodoacetamide, followed by trypsin digestion (Sequencing Grade Modified Trypsin, Promega Corp., Madison, WI) at  $37^\circ\text{C}$  for 4 hours in a Thermomixer with shaking (1000 rpm) at a substrate to enzyme ratio of 15:1 prior to acidification with 250 mM HCl (final concentration). Digested samples were stored at  $-80^\circ\text{C}$  until analysis.

**Chromatography:** Mass spectrometry and data analysis were performed as described below. These methods are an adaption of those described in (Zelter et al., 2015). Sample run order was randomized to minimize batch effects. For each injection, 3  $\mu$ L of digested protein was loaded by autosampler onto a 150- $\mu$ m Kasil fritted trap packed with 2 cm of Reprosil-Pur C18-AQ (3- $\mu$ m bead diameter, Dr. Maisch) at a flow rate of 2  $\mu$ L per min. After desalting with 8  $\mu$ L of 0.1% formic acid plus 2% acetonitrile, the trap was brought online with a Self-Packed PicoFrit Column (New Objective part number PF360-75-10-N-5, 75  $\mu$ m i.d.) packed with 30 cm of Reprosil-Pur C18-AQ (3- $\mu$ m bead diameter, Dr. Maisch) mounted to a heated nanospray ionization source (CorSolutions LLC, Ithaca, NY) set at  $50^\circ\text{C}$  and placed in line with a Thermo Scientific EASY-nLC 1200 UPLC pump plus autosampler.

Peptides were eluted from the column at 0.25  $\mu$ L/min using an acetonitrile gradient consisting of the following steps: (1) 0–10 mins; 6–10% B; (2) 10–90 mins; 10–32% B; (3) 100–130 mins; 32–75% B; (4) 130–135 mins; 75% B; (5) 135–136 mins; 75–100% B; (6) 136–151 mins; 100% B, followed by re-equilibration to 0% buffer B prior to the subsequent injection. Buffer A was: 0.1% formic acid in water and buffer B was 0.1% formic acid in acetonitrile.

**Data acquisition:** A Q Exactive HF-X (Thermo Fisher Scientific) was used to perform mass spectrometry in positive ion mode.

For cross-link identification experiments, data dependent acquisition (DDA) mode was used with a maximum of 20 tandem MS (MS/MS) spectra acquired per MS spectrum (scan range of  $m/z$  400–1,600). The resolution for MS and MS/MS was 60,000 at  $m/z$  200. Automatic gain control targets for MS and MS/MS were set to set to a nominal value of  $3e6$  and  $2e4$ , respectively, and maximum fill times were 50 and 100 ms, respectively. MS/MS spectra were acquired using an isolation width of 2  $m/z$  and a normalized collision energy of 27. MS/MS acquisitions were prevented for +1, +2, >+7 or undefined precursor charge states. Dynamic exclusion was set for 10 s. All spectra were collected in centroid mode.

For quantification experiments, single-injection data independent acquisition (DIA) runs were performed. MS spectra were acquired at 30,000 resolution with a scan range from 595 to 1205 m/z, automatic gain control of 3e6 and a maximum fill time of 45 ms. MS/MS spectra were acquired at 15,000 resolution using 8 m/z precursor isolation windows in a staggered-window pattern with optimized window placements from 600.5 to 1200.8m/z and a loop count of 75(Amodei et al., 2019). Automatic gain control was 1e6 and maximum fill time was 22 ms. All data were collected in centroid mode.

**DDA Data processing – identification of cross-linked peptides:** Acquired spectra were converted into mzML using ProteoWizard's msconvert(Chambers et al., 2012). All proteins in the sample were identified using Comet(Eng et al., 2013). Cross-linked peptides were identified within these proteins by Kojak version 2.0.0-dev available at (<http://www.kojak-ms.org>)(Hoopmann et al., 2015). A statistically meaningful q-value was assigned to each peptide spectrum match (PSM) through analysis of the target and decoy PSM distributions using Percolator version 2.08(Käll et al., 2007). Target databases consisted of all proteins identified in the sample analyzed. Decoy databases consisted of the corresponding set of reversed protein sequences. Data were filtered to show hits to the target proteins that had a Percolator assigned peptide level q-value < 0.01 and were identified by 2 or more PSMs. The complete unfiltered list of all PSMs and their Percolator assigned q-values are available on the ProXL web application at: <https://proxl.yeastrc.org/proxl/p/hhari> along with the raw MS spectra and search parameters used(Riffle et al., 2019, 2016).

Bibliospec DDA spectrum libraries for all Kojak searches were built using Skyline(Frewen et al., 2006; MacLean et al., 2010; Pino et al., 2020). For this purpose, Kojak results were converted to proxl XML format according to ProXL's instructions at [https://proxl-web-app.readthedocs.io/en/latest/using/upload\\_data.html](https://proxl-web-app.readthedocs.io/en/latest/using/upload_data.html). The resulting proxl XML file was input into Skyline's Bibliospec library builder. Cross-linked peptides identified by Kojak in DDA data were used to generate targets in Skyline for subsequent quantification of DIA data acquired on the same samples.

**DIA Data processing - quantification of cross-linked peptides:** DIA data were overlap demultiplexed with 10 ppm accuracy after peak picking in ProteoWizard (version 3.0.19014) prior to import into Skyline(Amodei et al., 2019). Peptides were quantified by integrating and summing the total fragment area of the most abundant 3 fragment ion transitions for each cross-linked peptide using Skyline(MacLean et al., 2010; Pino et al., 2020).

Ska core complex, spiked into all cross-linking reactions at 0.02 µg/µL, was used to normalize HHARI and 4EHP cross-linked peptides across all replicates. To this end, 4 cross-linked Ska core complex peptides were quantified, and their areas summed for each replicate. For each HHARI/4EHP cross-linked peptide the total fragment area of that peptide was divided by the Ska complex area sum for that replicate. For each individual cross-link, the most abundant peak area ratio was defined as 100% and values for the same cross-link in each replicate were calculated relative to this value. Full Skyline sessions are available on Panorama here: <https://panoramaweb.org/hhari.url>(Sharma et al., 2018).

**Co-elution size-exclusion chromatography**—Equimolar amounts (25  $\mu$ M) of HHARI and 4EHP were incubated for 10 minutes at room temperature before loading onto a Superdex 200 Increase 10/300 GL equilibrated in 25 mM Tris, 150 mM NaCl, 1 mM DTT pH 7.5 buffer. Peak fractions were analyzed by SDS-PAGE.

## QUANTIFICATION AND STATISTICAL ANALYSIS

Statistical significance of HDX-MS data was determined by a Welch's Student T-test, as described in (Hageman and Weis, 2019) for triplicate technical replicates. All peptides described as significant in the text or shown in figures have a significance cut-off of  $p < 0.01$ .

## Supplementary Material

Refer to Web version on PubMed Central for supplementary material.

## Acknowledgements:

We thank Lisa Tuttle for assistance with NMR analysis; Edgar Hodge and Mark Benhaim for assistance with HDX-MS data acquisition; Evie Henry for performing the cross-linking incubations and Lucas Murray for help analyzing the XL-MS data; and Sam Witus for proofreading the manuscript.

This research was supported by the National Institutes of Health under Awards R01 GM088055 (to R.E.K.), P41 GM103533 (to M.J.M.), F32 GM120797 (to K.H.R.), and R01AI153191 (to M.G.). R.E.K. is the Edmond H. Fischer/Washington Research Foundation Endowed Chair in Biochemistry.

## References

- Aguilera M, Oliveros M, Martínez-Padrón M, Barbas JA, Ferrús A, 2000. Ariadne-1: a vital *Drosophila* gene is required in development and defines a new conserved family of ring-finger proteins. *Genetics* 155, 1231–1244. 10.1093/genetics/155.3.1231 [PubMed: 10880484]
- Aguirre JD, Dunkerley KM, Lam R, Rusal M, Shaw GS, 2018. Impact of altered phosphorylation on loss of function of juvenile Parkinsonism-associated genetic variants of the E3 ligase parkin. *J. Biol. Chem* 293, 6337–6348. 10.1074/jbc.RA117.000605 [PubMed: 29530980]
- Aguirre JD, Dunkerley KM, Mercier P, Shaw GS, 2017. Structure of phosphorylated UBL domain and insights into PINK1-orchestrated parkin activation. *Proc. Natl. Acad. Sci. U. S. A* 114, 298–303. 10.1073/pnas.1613040114 [PubMed: 28007983]
- Amodei D, Egertson J, MacLean BX, Johnson R, Merrihew GE, Keller A, Marsh D, Vitek O, Mallick P, MacCoss MJ, 2019. Improving Precursor Selectivity in Data-Independent Acquisition Using Overlapping Windows. *J. Am. Soc. Mass Spectrom* 30, 669–684. 10.1007/s13361-018-2122-8 [PubMed: 30671891]
- Brzovic PS, Lissounov A, Christensen DE, Hoyt DW, Klevit RE, 2006. A UbcH5/ubiquitin noncovalent complex is required for processive BRCA1-directed ubiquitination. *Mol. Cell* 21, 873–880. 10.1016/j.molcel.2006.02.008 [PubMed: 16543155]
- Chambers MC, Maclean B, Burke R, Amodei D, Ruderman DL, Neumann S, Gatto L, Fischer B, Pratt B, Egertson J, Hoff K, Kessner D, Tasman N, Shulman N, Frewen B, Baker TA, Brusniak M-Y, Paulse C, Creasy D, Flashner L, Kani K, Moulding C, Seymour SL, Nuwaysir LM, Lefebvre B, Kuhlmann F, Roark J, Rainer P, Detlev S, Hemenway T, Huhmer A, Langridge J, Connolly B, Chadick T, Holly K, Eckels J, Deutsch EW, Moritz RL, Katz JE, Agus DB, MacCoss M, Tabb DL, Mallick P, 2012. A Cross-platform Toolkit for Mass Spectrometry and Proteomics. *Nat. Biotechnol* 30, 918–920. 10.1038/nbt.2377 [PubMed: 23051804]
- Condos TE, Dunkerley KM, Freeman EA, Barber KR, Aguirre JD, Chaugule VK, Xiao Y, Konermann L, Walden H, Shaw GS, 2018. Synergistic recruitment of UbcH7~Ub and phosphorylated Ubl domain triggers parkin activation. *EMBO J.* 37, e100014. 10.15252/embj.2018100014 [PubMed: 30446597]

- Cotton TR, Cobbold SA, Bernardini JP, Richardson LW, Wang XS, Lechtenberg BC, 2021. Structural basis of K63-ubiquitin chain formation by the Gordon-Holmes syndrome RBR E3 ubiquitin ligase RNF216. *Mol. Cell* 1097–2765(21)01067–4. 10.1016/j.molcel.2021.12.005
- Cotton TR, Lechtenberg BC, 2020. Chain reactions: molecular mechanisms of RBR ubiquitin ligases. *Biochem. Soc. Trans* 48, 1737–1750. 10.1042/BST20200237 [PubMed: 32677670]
- Cowan AD, Ciulli A, 2022. Driving E3 Ligase Substrate Specificity for Targeted Protein Degradation: Lessons from Nature and the Laboratory. *Annu. Rev. Biochem* 10.1146/annurev-biochem-032620-104421
- Delaglio F, Grzesiek S, Vuister GW, Zhu G, Pfeifer J, Bax A, 1995. NMRPipe: a multidimensional spectral processing system based on UNIX pipes. *J. Biomol. NMR* 6, 277–293. 10.1007/BF00197809 [PubMed: 8520220]
- Dove KK, Kemp HA, Bona KRD, Reiter KH, Milburn LJ, Camacho D, Fay DS, Miller DL, Klevit RE, 2017a. Two functionally distinct E2/E3 pairs coordinate sequential ubiquitination of a common substrate in *Caenorhabditis elegans* development. *Proc. Natl. Acad. Sci* 114, E6576–E6584. 10.1073/pnas.1705060114 [PubMed: 28739890]
- Dove KK, Klevit RE, 2017. RING-Between-RING E3 Ligases: Emerging Themes amid the Variations. *J. Mol. Biol* 429, 3363–3375. 10.1016/j.jmb.2017.08.008 [PubMed: 28827147]
- Dove KK, Olszewski JL, Martino L, Duda DM, Wu XS, Miller DJ, Reiter KH, Rittinger K, Schulman BA, Klevit RE, 2017b. Structural Studies of HHARI/UbcH7~Ub Reveal Unique E2~Ub Conformational Restriction by RBR RING1. *Struct. Lond. Engl* 1993 25, 890–900.e5. 10.1016/j.str.2017.04.013
- Dove KK, Stieglitz B, Duncan ED, Rittinger K, Klevit RE, 2016. Molecular insights into RBR E3 ligase ubiquitin transfer mechanisms. *EMBO Rep.* 17, 1221–1235. 10.15252/embr.201642641 [PubMed: 27312108]
- Duda DM, Olszewski JL, Schuermann JP, Kurinov I, Miller DJ, Nourse A, Alpi AF, Schulman BA, 2013. Structure of HHARI, a RING-IBR-RING ubiquitin ligase: autoinhibition of an Ariadne-family E3 and insights into ligation mechanism. *Struct. Lond. Engl* 1993 21, 1030–1041. 10.1016/j.str.2013.04.019
- Eiyama A, Okamoto K, 2015. PINK1/Parkin-mediated mitophagy in mammalian cells. *Curr. Opin. Cell Biol* 33, 95–101. 10.1016/j.ceb.2015.01.002 [PubMed: 25697963]
- Elmehdawi F, Whewey G, Szymanska K, Adams M, High AS, Johnson CA, Robinson PA, 2013. Human Homolog of *Drosophila* Ariadne (HHARI) is a marker of cellular proliferation associated with nuclear bodies. *Exp. Cell Res* 319, 161–172. 10.1016/j.yexcr.2012.10.002 [PubMed: 23059369]
- Eng JK, Jahan TA, Hoopmann MR, 2013. Comet: an open-source MS/MS sequence database search tool. *Proteomics* 13, 22–24. 10.1002/pmic.201200439 [PubMed: 23148064]
- Engen JR, 2009. Analysis of protein conformation and dynamics by hydrogen/deuterium exchange MS. *Anal. Chem* 81, 7870–7875. 10.1021/ac901154s [PubMed: 19788312]
- Faull SV, Lau AMC, Martens C, Ahdash Z, Hansen K, Yebenes H, Schmidt C, Beuron F, Cronin NB, Morris EP, Politis A, 2019. Structural basis of Cullin 2 RING E3 ligase regulation by the COP9 signalosome. *Nat. Commun* 10, 3814. 10.1038/s41467-019-11772-y [PubMed: 31444342]
- Frewen BE, Merrihew GE, Wu CC, Noble WS, MacCoss MJ, 2006. Analysis of peptide MS/MS spectra from large-scale proteomics experiments using spectrum libraries. *Anal. Chem* 78, 5678–5684. 10.1021/ac060279n [PubMed: 16906711]
- Gladkova C, Maslen SL, Skehel JM, Komander D, 2018. Mechanism of parkin activation by PINK1. *Nature* 559, 410–414. 10.1038/s41586-018-0224-x [PubMed: 29995846]
- Gradilla A-C, Mansilla A, Ferrús A, 2011. Isoform-specific regulation of a steroid hormone nuclear receptor by an E3 ubiquitin ligase in *Drosophila melanogaster*. *Genetics* 189, 871–883. 10.1534/genetics.111.132191 [PubMed: 21900267]
- Haas TL, Emmerich CH, Gerlach B, Schmukle AC, Cordier SM, Rieser E, Feltham R, Vince J, Warnken U, Wenger T, Koschny R, Komander D, Silke J, Walczak H, 2009. Recruitment of the linear ubiquitin chain assembly complex stabilizes the TNF-R1 signaling complex and is required for TNF-mediated gene induction. *Mol. Cell* 36, 831–844. 10.1016/j.molcel.2009.10.013 [PubMed: 20005846]

- Hageman TS, Weis DD, 2019. Reliable Identification of Significant Differences in Differential Hydrogen Exchange-Mass Spectrometry Measurements Using a Hybrid Significance Testing Approach. *Anal. Chem* 91, 8008–8016. 10.1021/acs.analchem.9b01325 [PubMed: 31099554]
- Hart T, Chandrashekar M, Aregger M, Steinhart Z, Brown KR, MacLeod G, Mis M, Zimmermann M, Fradet-Turcotte A, Sun S, Mero P, Dirks P, Sidhu S, Roth FP, Rissland OS, Durocher D, Angers S, Moffat J, 2015. High-Resolution CRISPR Screens Reveal Fitness Genes and Genotype-Specific Cancer Liabilities. *Cell* 163, 1515–1526. 10.1016/j.cell.2015.11.015 [PubMed: 26627737]
- Helgeson LA, Zelter A, Riffle M, MacCoss MJ, Asbury CL, Davis TN, 2018. Human Ska complex and Ndc80 complex interact to form a load-bearing assembly that strengthens kinetochore-microtubule attachments. *Proc. Natl. Acad. Sci. U. S. A* 115, 2740–2745. 10.1073/pnas.1718553115 [PubMed: 29487209]
- Honorato RV, Koukos PI, Jiménez-García B, Tsaregorodtsev A, Verlato M, Giachetti A, Rosato A, Bonvin AMJJ, 2021. Structural Biology in the Clouds: The WeNMR-EOSC Ecosystem. *Front. Mol. Biosci* 8, 708. 10.3389/fmolb.2021.729513
- Hoopmann MR, Zelter A, Johnson RS, Riffle M, MacCoss MJ, Davis TN, Moritz RL, 2015. Kojak: efficient analysis of chemically cross-linked protein complexes. *J. Proteome Res* 14, 2190–2198. 10.1021/pr501321h [PubMed: 25812159]
- Horn-Ghetko D, Krist DT, Prabu JR, Baek K, Mulder MPC, Klügel M, Scott DC, Ovaas H, Kleiger G, Schulman BA, 2021. Ubiquitin ligation to F-box protein targets by SCF-RBR E3-E3 super-assembly. *Nature* 590, 671–676. 10.1038/s41586-021-03197-9 [PubMed: 33536622]
- Iconomou M, Saunders DN, 2016. Systematic approaches to identify E3 ligase substrates. *Biochem. J* 473, 4083–4101. 10.1042/BCJ20160719 [PubMed: 27834739]
- Iwai K, Fujita H, Sasaki Y, 2014. Linear ubiquitin chains: NF- $\kappa$ B signalling, cell death and beyond. *Nat. Rev. Mol. Cell Biol* 15, 503–508. 10.1038/nrm3836 [PubMed: 25027653]
- Jevtić P, Haakonsen DL, Rapé M, 2021. An E3 ligase guide to the galaxy of small-molecule-induced protein degradation. *Cell Chem. Biol* 28, 1000–1013. 10.1016/j.chembiol.2021.04.002 [PubMed: 33891901]
- Käll L, Canterbury JD, Weston J, Noble WS, MacCoss MJ, 2007. Semi-supervised learning for peptide identification from shotgun proteomics datasets. *Nat. Methods* 4, 923–925. 10.1038/nmeth1113 [PubMed: 17952086]
- Kelsall IR, Duda DM, Olszewski JL, Hofmann K, Knebel A, Langevin F, Wood N, Wightman M, Schulman BA, Alpi AF, 2013. TRIAD1 and HHARI bind to and are activated by distinct neddylated Cullin-RING ligase complexes. *EMBO J.* 32, 2848–2860. 10.1038/emboj.2013.209 [PubMed: 24076655]
- Kumar A, Aguirre JD, Condos TEC, Martinez-Torres RJ, Chaugule VK, Toth R, Sundaramoorthy R, Mercier P, Knebel A, Spratt DE, Barber KR, Shaw GS, Walden H, 2015. Disruption of the autoinhibited state primes the E3 ligase parkin for activation and catalysis. *EMBO J.* 34, 2506–2521. 10.15252/embj.201592337 [PubMed: 26254304]
- Lechtenberg BC, Rajput A, Sanishvili R, Dobaczewska MK, Ware CF, Mace PD, Riedl SJ, 2016. Structure of a HOIP/E2-ubiquitin complex reveals RBR E3 ligase mechanism and regulation. *Nature* 529, 546–550. 10.1038/nature16511 [PubMed: 26789245]
- Liu J, Wang Y, Gong Y, Fu T, Hu S, Zhou Z, Pan L, 2017. Structural Insights into SHARPIN-Mediated Activation of HOIP for the Linear Ubiquitin Chain Assembly. *Cell Rep.* 21, 27–36. 10.1016/j.celrep.2017.09.031 [PubMed: 28978479]
- MacLean B, Tomazela DM, Shulman N, Chambers M, Finney GL, Frewen B, Kern R, Tabb DL, Liebler DC, MacCoss MJ, 2010. Skyline: an open source document editor for creating and analyzing targeted proteomics experiments. *Bioinforma. Oxf. Engl* 26, 966–968. 10.1093/bioinformatics/btq054
- Marley J, Lu M, Bracken C, 2001. A method for efficient isotopic labeling of recombinant proteins. *J. Biomol. NMR* 20, 71–75. 10.1023/a:1011254402785 [PubMed: 11430757]
- Masson GR, Burke JE, Ahn NG, Anand GS, Borchers C, Brier S, Bou-Assaf GM, Engen JR, Englander SW, Faber J, Garlish R, Griffin PR, Gross ML, Guttman M, Hamuro Y, Heck AJR, Houde D, Jacob RE, Jørgensen TJD, Kaltashov IA, Klinman JP, Konermann L, Man P, Mayne L, Pascal BD, Reichmann D, Skehel M, Snijder J, Strutzenberg TS, Underbakke ES, Wagner

- C, Wales TE, Walters BT, Weis DD, Wilson DJ, Wintrobe PL, Zhang Z, Zheng J, Schriemer DC, Rand KD, 2019. Recommendations for performing, interpreting and reporting hydrogen deuterium exchange mass spectrometry (HDX-MS) experiments. *Nat. Methods* 16, 595–602. 10.1038/s41592-019-0459-y [PubMed: 31249422]
- Merkley ED, Rysavy S, Kahraman A, Hafen RP, Daggett V, Adkins JN, 2014. Distance restraints from crosslinking mass spectrometry: mining a molecular dynamics simulation database to evaluate lysine-lysine distances. *Protein Sci. Publ. Protein Soc* 23, 747–759. 10.1002/pro.2458
- Mertins P, Yang F, Liu T, Mani DR, Petyuk VA, Gillette MA, Clauser KR, Qiao JW, Gritsenko MA, Moore RJ, Levine DA, Townsend R, Erdmann-Gilmore P, Snider JE, Davies SR, Ruggles KV, Fenyo D, Kitchens RT, Li S, Olvera N, Dao F, Rodriguez H, Chan DW, Liebler D, White F, Rodland KD, Mills GB, Smith RD, Paulovich AG, Ellis M, Carr SA, 2014. Ischemia in tumors induces early and sustained phosphorylation changes in stress kinase pathways but does not affect global protein levels. *Mol. Cell. Proteomics MCP* 13, 1690–1704. 10.1074/mcp.M113.036392 [PubMed: 24719451]
- Ordureau A, Heo J-M, Duda DM, Paulo JA, Olszewski JL, Yanishevski D, Rinehart J, Schulman BA, Harper JW, 2015. Defining roles of PARKIN and ubiquitin phosphorylation by PINK1 in mitochondrial quality control using a ubiquitin replacement strategy. *Proc. Natl. Acad. Sci. U. S. A* 112, 6637–6642. 10.1073/pnas.1506593112 [PubMed: 25969509]
- Peacock RB, Komives EA, 2021. Hydrogen/Deuterium Exchange and Nuclear Magnetic Resonance Spectroscopy Reveal Dynamic Allostery on Multiple Time Scales in the Serine Protease Thrombin. *Biochemistry* 60, 3441–3448. 10.1021/acs.biochem.1c00277 [PubMed: 34159782]
- Peter D, Weber R, Sandmeir F, Wohlbold L, Helms S, Bawankar P, Valkov E, Igreja C, Izaurralde E, 2017. GIGYF1/2 proteins use auxiliary sequences to selectively bind to 4EHP and repress target mRNA expression. *Genes Dev.* 31, 1147–1161. 10.1101/gad.299420.117 [PubMed: 28698298]
- Pickrell AM, Youle RJ, 2015. The roles of PINK1, parkin, and mitochondrial fidelity in Parkinson's disease. *Neuron* 85, 257–273. 10.1016/j.neuron.2014.12.007 [PubMed: 25611507]
- Pino LK, Searle BC, Bollinger JG, Nunn B, MacLean B, MacCoss MJ, 2020. The Skyline ecosystem: Informatics for quantitative mass spectrometry proteomics. *Mass Spectrom. Rev* 39, 229–244. 10.1002/mas.21540 [PubMed: 28691345]
- Poush JA, Blouin NA, Di Bona KR, Lažeti V, Fay DS, 2018. Regulation of germ cell development by ARI1 family ubiquitin ligases in *C. elegans*. *Sci. Rep* 8, 17737. 10.1038/s41598-018-35691-y [PubMed: 30531803]
- Qiu X, Fay DS, 2006. ARI-1, an RBR family ubiquitin-ligase, functions with UBC-18 to regulate pharyngeal development in *C. elegans*. *Dev. Biol* 291, 239–252. 10.1016/j.ydbio.2005.11.045 [PubMed: 16457801]
- Ramirez-Sarmiento CA, Komives EA, 2018. Hydrogen-deuterium exchange mass spectrometry reveals folding and allostery in protein-protein interactions. *Methods San Diego Calif* 144, 43–52. 10.1016/j.ymeth.2018.04.001
- Riffle M, Jaschob D, Zelter A, Davis TN, 2019. Prox1 (Protein Cross-Linking Database): A Public Server, QC Tools, and Other Major Updates. *J. Proteome Res* 18, 759–764. 10.1021/acs.jproteome.8b00726 [PubMed: 30525651]
- Riffle M, Jaschob D, Zelter A, Davis TN, 2016. ProXL (Protein Cross-Linking Database): A Platform for Analysis, Visualization, and Sharing of Protein Cross-Linking Mass Spectrometry Data. *J. Proteome Res* 15, 2863–2870. 10.1021/acs.jproteome.6b00274 [PubMed: 27302480]
- Riley BE, Loughheed JC, Callaway K, Velasquez M, Brecht E, Nguyen L, Shaler T, Walker D, Yang Y, Regnstrom K, Diep L, Zhang Z, Chiou S, Bova M, Artis DR, Yao N, Baker J, Yednock T, Johnston JA, 2013. Structure and function of Parkin E3 ubiquitin ligase reveals aspects of RING and HECT ligases. *Nat. Commun* 4, 1982. 10.1038/ncomms2982 [PubMed: 23770887]
- Sauvé V, Lilov A, Seirafi M, Vranas M, Rasool S, Kozlov G, Sprules T, Wang J, Trempe J-F, Gehring K, 2015. A Ubl/ubiquitin switch in the activation of Parkin. *EMBO J.* 34, 2492–2505. 10.15252/embj.201592237 [PubMed: 26254305]
- Sauvé V, Sung G, Soya N, Kozlov G, Blaimschein N, Miotto LS, Trempe J-F, Lukacs GL, Gehring K, 2018. Mechanism of parkin activation by phosphorylation. *Nat. Struct. Mol. Biol* 25, 623–630. 10.1038/s41594-018-0088-7 [PubMed: 29967542]

- Scott DC, Rhee DY, Duda DM, Kelsall IR, Olszewski JL, Paulo JA, de Jong A, Ovaas H, Alpi AF, Harper JW, Schulman BA, 2016. Two Distinct Types of E3 Ligases Work in Unison to Regulate Substrate Ubiquitylation. *Cell* 166, 1198–1214.e24. 10.1016/j.cell.2016.07.027 [PubMed: 27565346]
- Seenivasan R, Hermanns T, Blyszcz T, Lammers M, Praefcke GJK, Hofmann K, 2019. Mechanism and chain specificity of RNF216/TRIAD3, the ubiquitin ligase mutated in Gordon Holmes syndrome. *Hum. Mol. Genet* 28, 2862–2873. 10.1093/hmg/ddz098 [PubMed: 31087003]
- Sharma V, Eckels J, Schilling B, Ludwig C, Jaffe JD, MacCoss MJ, MacLean B, 2018. Panorama Public: A Public Repository for Quantitative Data Sets Processed in Skyline. *Mol. Cell. Proteomics MCP* 17, 1239–1244. 10.1074/mcp.RA117.000543 [PubMed: 29487113]
- Spratt DE, Mercier P, Shaw GS, 2013. Structure of the HHARI catalytic domain shows glimpses of a HECT E3 ligase. *PLoS One* 8, e74047. 10.1371/journal.pone.0074047 [PubMed: 24058416]
- Stieglitz B, Rana RR, Koliopoulos MG, Morris-Davies AC, Schaeffer V, Christodoulou E, Howell S, Brown NR, Dikic I, Rittinger K, 2013. Structural basis for ligase-specific conjugation of linear ubiquitin chains by HOIP. *Nature* 503, 422–426. 10.1038/nature12638 [PubMed: 24141947]
- Swatek KN, Komander D, 2016. Ubiquitin modifications. *Cell Res.* 26, 399–422. 10.1038/cr.2016.39 [PubMed: 27012465]
- Tan KL, Haelterman NA, Kwartler CS, Regalado ES, Lee P-T, Nagarkar-Jaiswal S, Guo D-C, Duraine L, Wangler MF, University of Washington Center for Mendelian Genomics, Bamshad MJ, Nickerson DA, Lin G, Milewicz DM, Bellen HJ, 2018. Ari-1 Regulates Myonuclear Organization Together with Parkin and Is Associated with Aortic Aneurysms. *Dev. Cell* 45, 226–244.e8. 10.1016/j.devcel.2018.03.020 [PubMed: 29689197]
- Tan NGS, Ardley HC, Scott GB, Rose SA, Markham AF, Robinson PA, 2003. Human homologue of Ariadne promotes the ubiquitylation of translation initiation factor 4E homologous protein, 4EHP. *FEBS Lett.* 554, 501–504. 10.1016/s0014-5793(03)01235-3 [PubMed: 14623119]
- Trempe J-F, Sauvé V, Grenier K, Seirafi M, Tang MY, Ménade M, Al-Abdul-Wahid S, Krett J, Wong K, Kozlov G, Nagar B, Fon EA, Gehring K, 2013. Structure of parkin reveals mechanisms for ubiquitin ligase activation. *Science* 340, 1451–1455. 10.1126/science.1237908 [PubMed: 23661642]
- van Zundert GCP, Rodrigues JPGLM, Trellet M, Schmitz C, Kastrius PL, Karaca E, Melquiond ASJ, van Dijk M, de Vries SJ, Bonvin AMJJ, 2016. The HADDOCK2.2 Web Server: User-Friendly Integrative Modeling of Biomolecular Complexes. *J. Mol. Biol., Computation Resources for Molecular Biology* 428, 720–725. 10.1016/j.jmb.2015.09.014
- Vizcaíno JA, Côté R, Reisinger F, M. Foster J, Mueller M, Rameseder J, Hermjakob H, Martens L, 2009. A guide to the Proteomics Identifications Database proteomics data repository. *Proteomics* 9, 4276–4283. 10.1002/pmic.200900402 [PubMed: 19662629]
- von Stechow L, Typas D, Carreras Puigvert J, Oort L, Siddappa R, Pines A, Vrieling H, van de Water B, Mullenders LHF, Danen EHJ, 2015. The E3 ubiquitin ligase ARIH1 protects against genotoxic stress by initiating a 4EHP-mediated mRNA translation arrest. *Mol. Cell. Biol* 35, 1254–1268. 10.1128/MCB.01152-14 [PubMed: 25624349]
- Wang T, Birsoy K, Hughes NW, Krupczak KM, Post Y, Wei JJ, Lander ES, Sabatini DM, 2015. Identification and characterization of essential genes in the human genome. *Science* 350, 1096–1101. 10.1126/science.aac7041 [PubMed: 26472758]
- Watson MJ, Harkewicz R, Hodge EA, Vorauer C, Palmer J, Lee KK, Guttman M, 2021. Simple Platform for Automating Decoupled LC-MS Analysis of Hydrogen/Deuterium Exchange Samples. *J. Am. Soc. Mass Spectrom* 32, 597–600. 10.1021/jasms.0c00341 [PubMed: 33284630]
- Wenzel DM, Lissounov A, Brzovic PS, Klevit RE, 2011. UBCH7 reactivity profile reveals parkin and HHARI to be RING/HECT hybrids. *Nature* 474, 105–108. 10.1038/nature09966 [PubMed: 21532592]
- Yuan L, Lv Z, Atkison JH, Olsen SK, 2017. Structural insights into the mechanism and E2 specificity of the RBR E3 ubiquitin ligase HHARI. *Nat. Commun* 8, 211. 10.1038/s41467-017-00272-6 [PubMed: 28790309]
- Zelter A, Bonomi M, Kim JO, Umbreit NT, Hoopmann MR, Johnson R, Riffle M, Jaschob D, MacCoss MJ, Moritz RL, Davis TN, 2015. The molecular architecture of the Dam1 kinetochore

complex is defined by cross-linking based structural modelling. Nat. Commun 6, 8673. 10.1038/ncomms9673 [PubMed: 26560693]

Author Manuscript

Author Manuscript

Author Manuscript

Author Manuscript

### Highlights

- A phosphomimetic mutation in the HHARI Ariadne domain releases auto-inhibition.
- The HHARI Rcat domain contains a substrate binding surface.
- Domain rearrangements induced by activation and E3 complex formation are revealed.

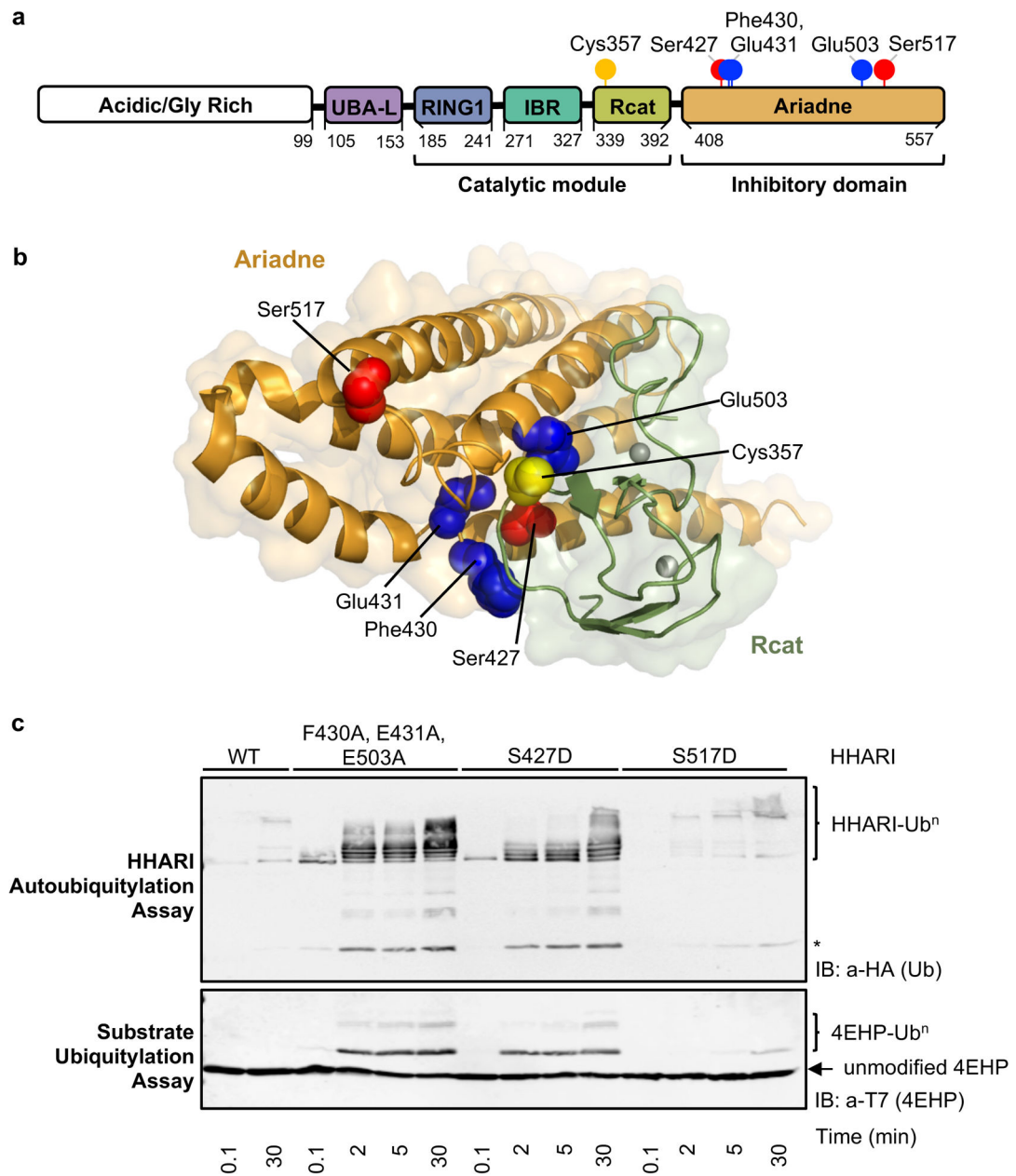


**Figure 1. HHARI phosphomimetic activation**

(A) HHARI domain organization. The location of Rcat catalytic cysteine (C357), structural activation residues (F430, E431, E503), and phospho-sites (S427, S517) are shown as spheres (yellow, blue, and red, respectively). (B) Residues described in (A) are mapped onto the Rcat-Ariadne surface of auto-inhibited HHARI (PDB: 4KC9). (C) HHARI reactivity assays in the absence (auto-ubiquitylation, top panel) and presence of 4EHP substrate (bottom panel). See also Figure S1.

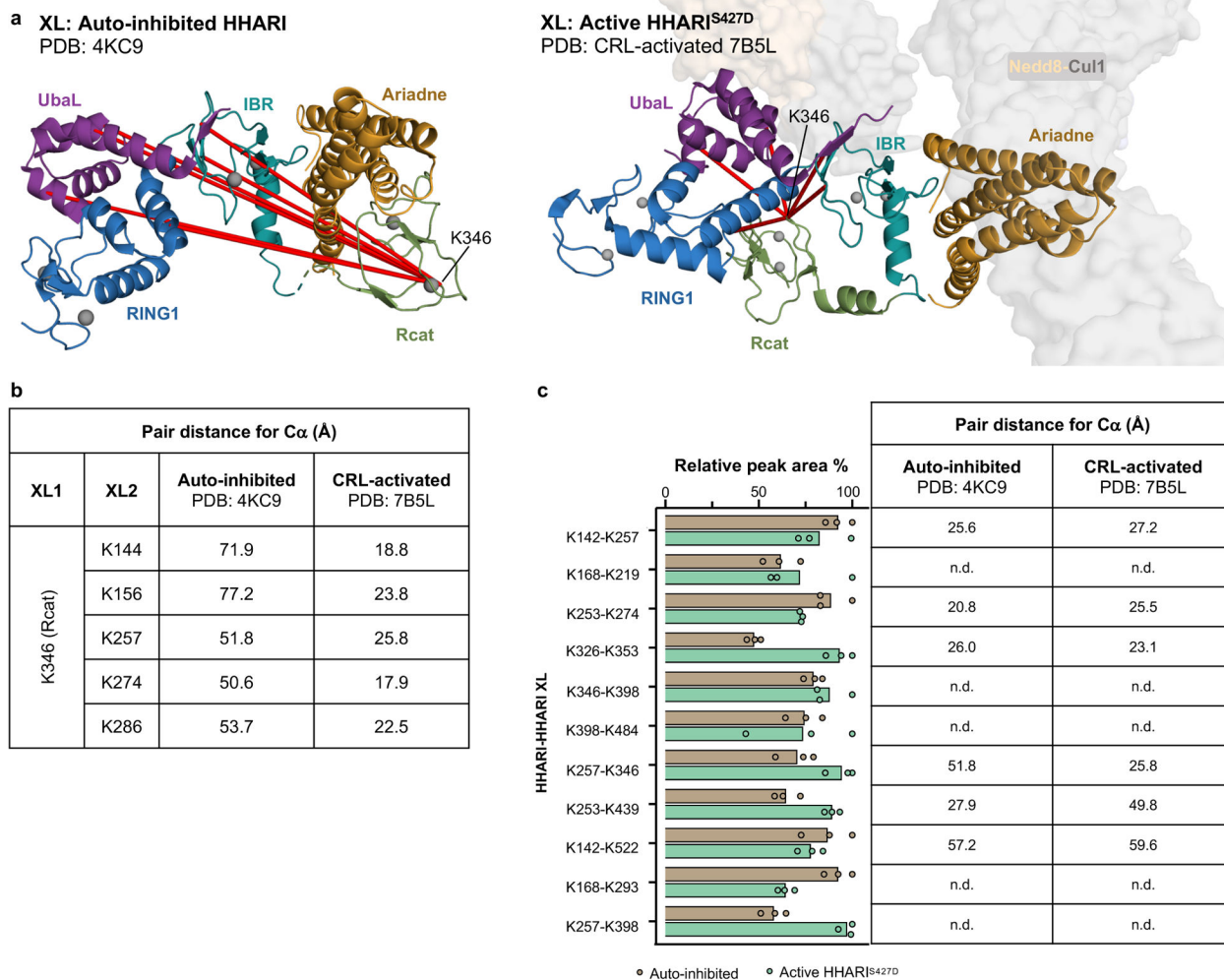


### Figure 2. Rcat domain rearrangements revealed by cross-linking MS

A) Cross-links observed in auto-inhibited and HHARI<sup>S427D</sup> samples emanating between Rcat residue K346 and N-terminal domains (UbaL, RING1) are mapped onto auto-inhibited (PDB: 4KC9) and CRL-activated (PDB: 7B5L) HHARI structures, respectively. Scaffolding CRL complex components (Nedd8-Cul1) are shown as surface representations. (B) C $\alpha$ -C $\alpha$  distances from atomic structures are reported for cross-links shown in (A). (C) Relative peak area percent of quantified intra-HHARI DSS crosslinks. Results are expressed as averages, overlaid with individual points from triplicate experiments. C $\alpha$ -C $\alpha$  distances from atomic structures are reported for quantified cross-links. Distances for pairs lacking structural resolution were not determined (n.d.). See also Figure S2.

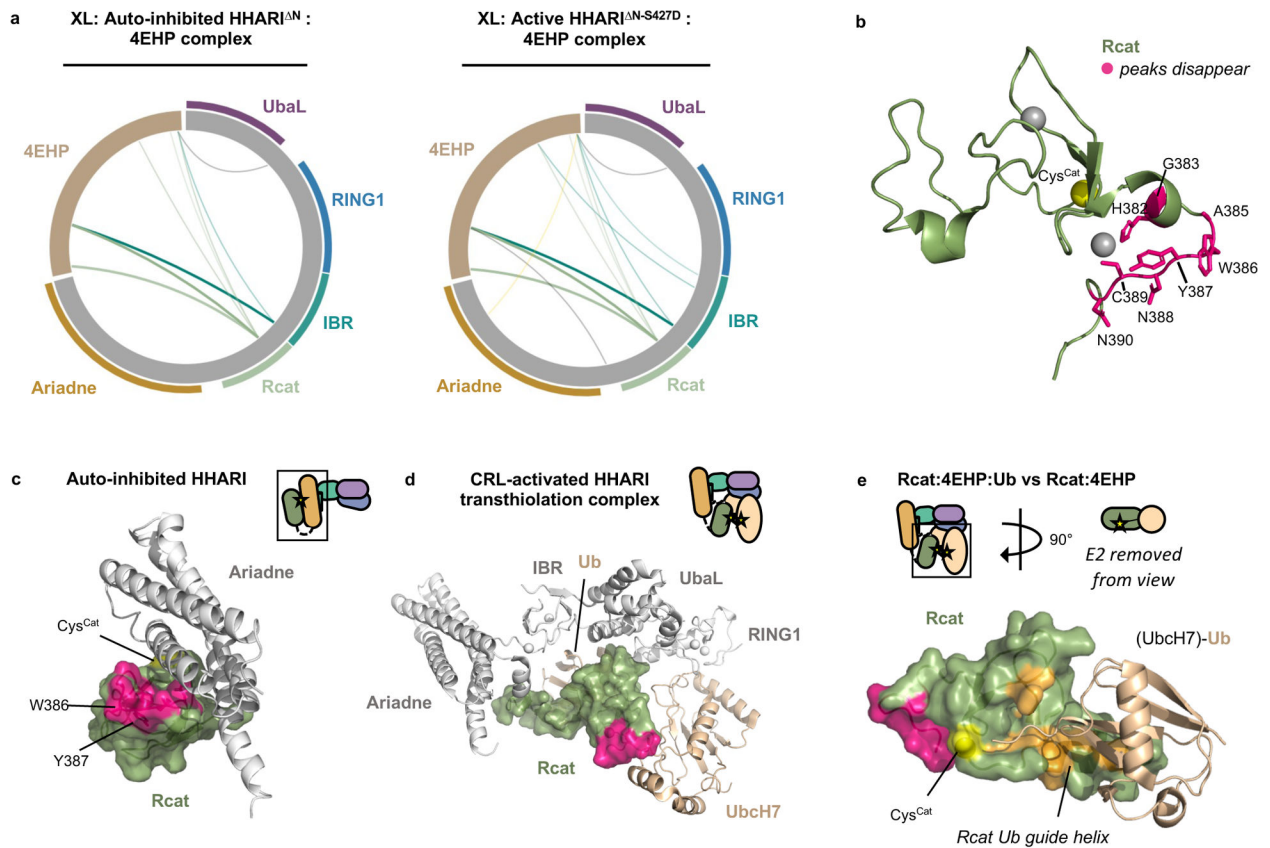


### Figure 3. HHARI Rcat domain binds substrate

(A) Circle plot of inter-molecular DSS cross-links identified in HHARI-4EHP complexes. Line colors correspond to HHARI domains as shown on the perimeter of each circle, with widths relative to number of peptide spectrum matches (PSM) identified. Cross-links identified in all three replicates are shown. (B) Residues broadened in  $^1\text{H}$ ,  $^{15}\text{N}$ -TROSY NMR spectra of  $^{15}\text{N}$ -Rcat in the presence of 4EHP (pink) are mapped onto the surface of Rcat (PDB: 2M9Y). (C) Residues identified in (B) are mapped onto the auto-inhibited (PDB: 4KC9) and (D) CRL-activated (PDB: 7B5L) HHARI structures. The Rcat surface represents the construct used for NMR studies. (E) Residues broadened in  $^1\text{H}$ ,  $^{15}\text{N}$ -TROSY NMR spectra of  $^{15}\text{N}$ -Rcat-4EHP complex in the presence of Ub are mapped onto the surface of Rcat (orange) extracted from the CRL-activated transthiolation HHARI complex (PDB:7B5L). UbcH7 has been removed from this view to better display Ub interactions with Rcat. See also Figure S3.

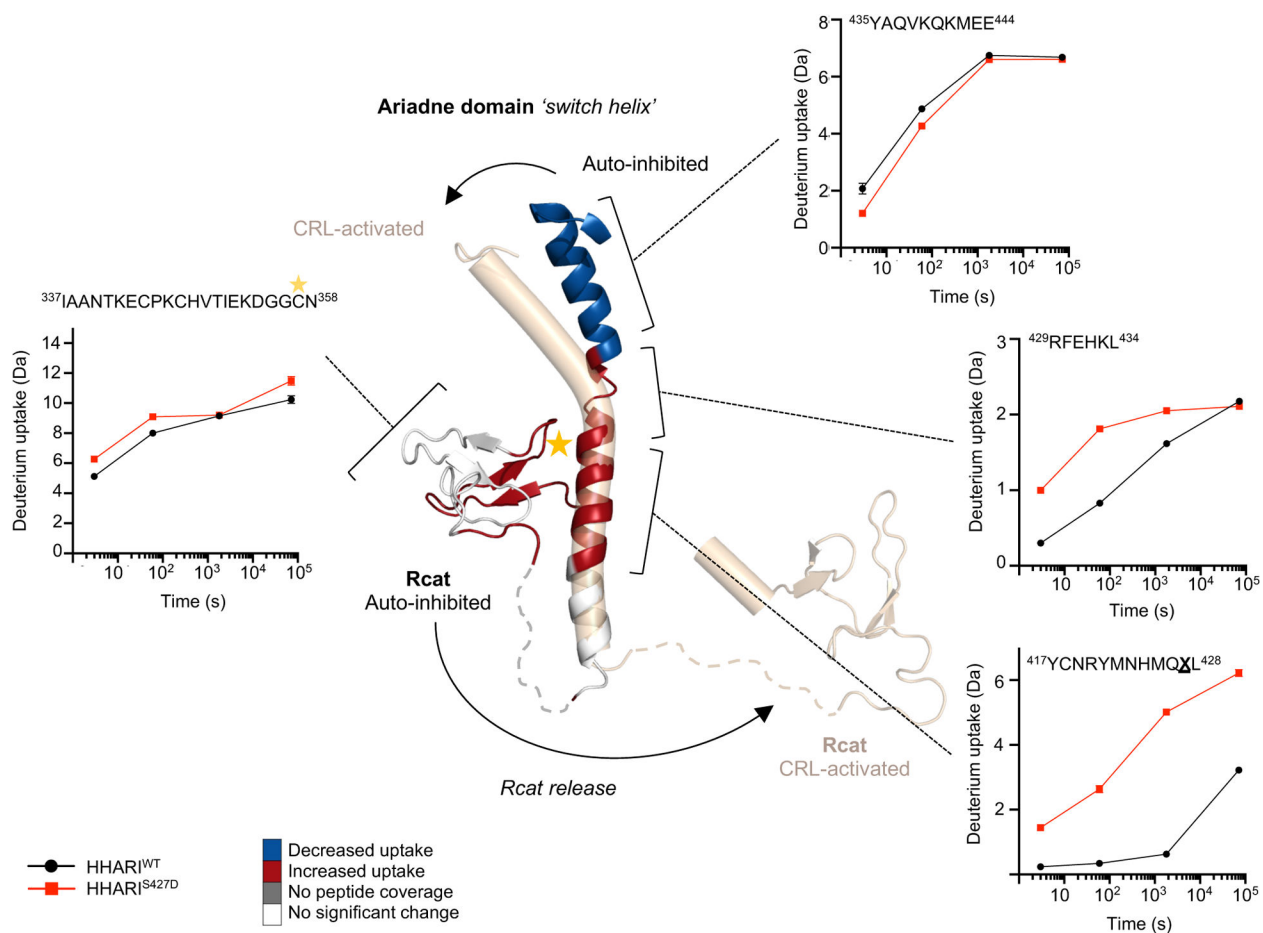


#### Figure 4. Ariadne phospho-mimetic disrupts the Rcat interface

Difference in deuterium uptake between HHARI and HHARI<sup>S427D</sup> is plotted onto auto-inhibited Rcat and Ariadne helix1 (switch helix) (PDB: 4KC9, helical cartoon). Data from the 3 s timepoint are shown; significant peptides (significance cut-offs  $p < 0.01$  and  $\text{HDX} > 0.4$  Da from Welch's T test and CI) with decreased or increased deuterium uptake are shown as blue or red, respectively. The corresponding region of CRL-activated HHARI is aligned to the distal start of the switch helix and displayed as a solid wheat cylinder. The release of Rcat from the auto-inhibited Ariadne interface upon interaction with Nedd8-Cul1-Rbx1 is shown. Representative HDX uptake plots are shown for affected peptides. Each data point represents the mean of 3 experimental replicates, with error bars  $\pm$  SD. The Rcat catalytic cysteine is noted with a yellow star in peptide 337–358.

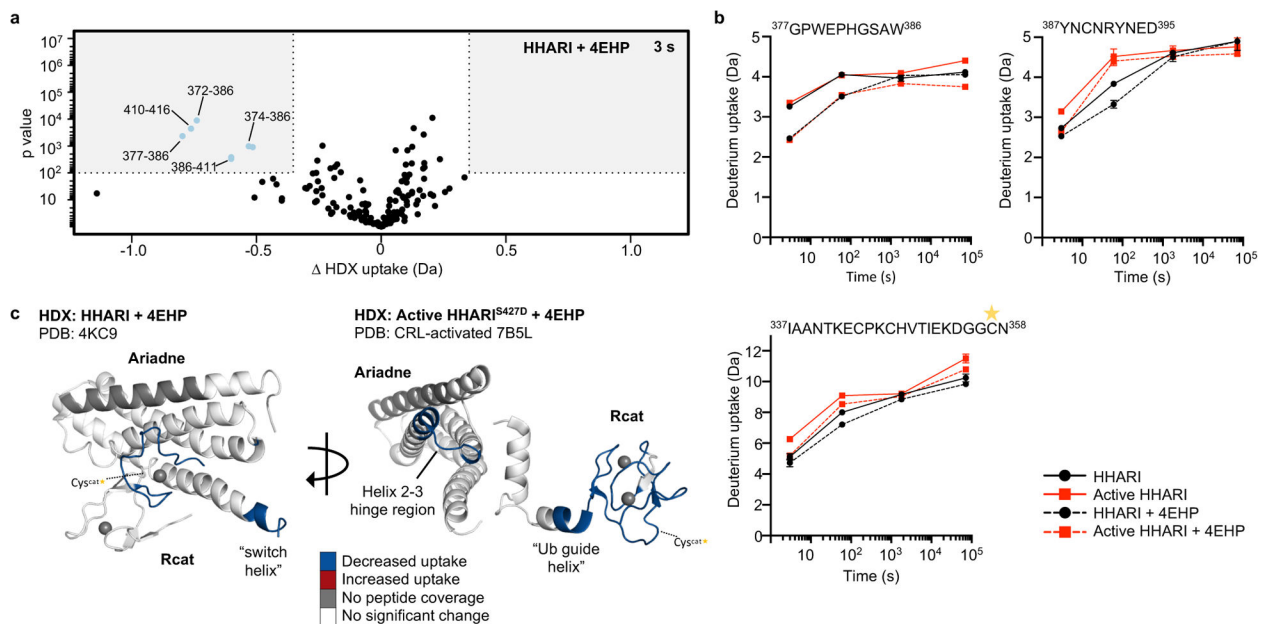


**Figure 5. 4EHP binding protects Rcat**

(A) Volcano plot comparison of change in deuterium uptake of HHARI peptides due to 4EHP binding. Data plotted are for the 3 s timepoint (significance cut-offs  $p < 0.01$  and  $\text{HDX} > 0.35$  Da from Welch's T test and Critical interval). Significant peptides are colored blue. (B) Representative HDX uptake plots are shown for affected peptides from HHARI and phosphomimetic complexes. Each data point represents the mean of 3 experimental replicates, with error bars  $\pm$  SD. (C) Change in deuterium uptake of HHARI peptides at 3 s between HHARI- and HHARI<sup>S427D</sup>-bound 4EHP complexes are plotted onto respective Rcat-Ariadne domains (auto-inhibited PDB: 4KC9, CRL-activated PDB: 7B5L).

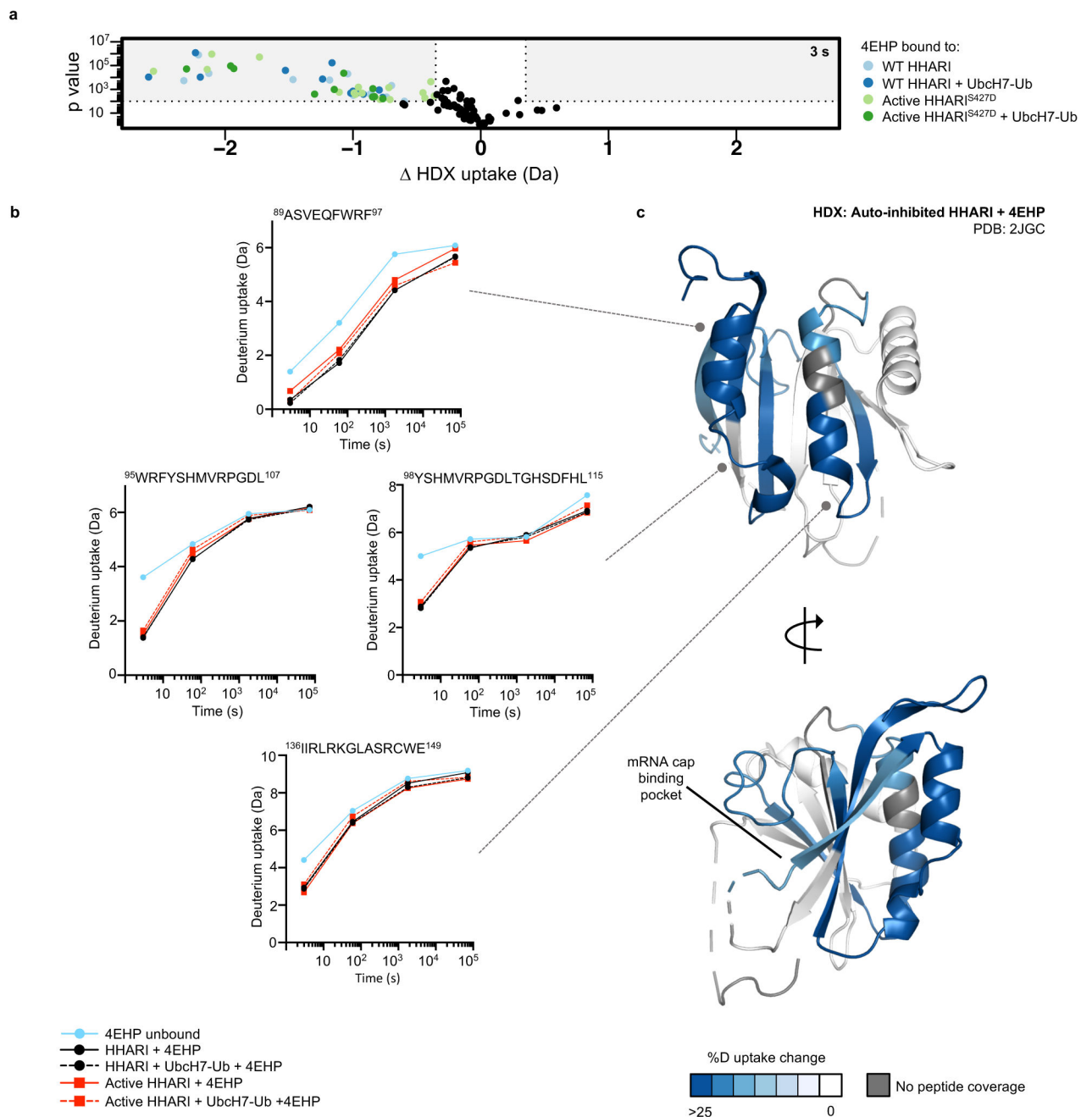


### Figure 6. 4EHP surface involved in HHARI binding

(A) Volcano plot comparison of change in deuterium uptake of 4EHP peptides due to HHARI, or HHARI + Ubch7-Ub binding at 3 s ( $p < 0.01$ ). (B) Representative HDX uptake plots are shown for affected 4EHP peptides from 4EHP and HHARI complexes. Each data point represents the mean of 3 experimental replicates, with error bars  $\pm$  SD. (C) Change in HDX at 3 s (significance cut-offs  $p < 0.01$  and  $\Delta \text{HDX} > 0.35$  Da from Welch's T test and Critical interval) between 4EHP and HHARI complexes are plotted onto 4EHP (PDB:2JGC). Protected peptides are shaded blue by percent change in deuterium uptake. The location of the 4EHP mRNA 5' cap binding pocket is noted.

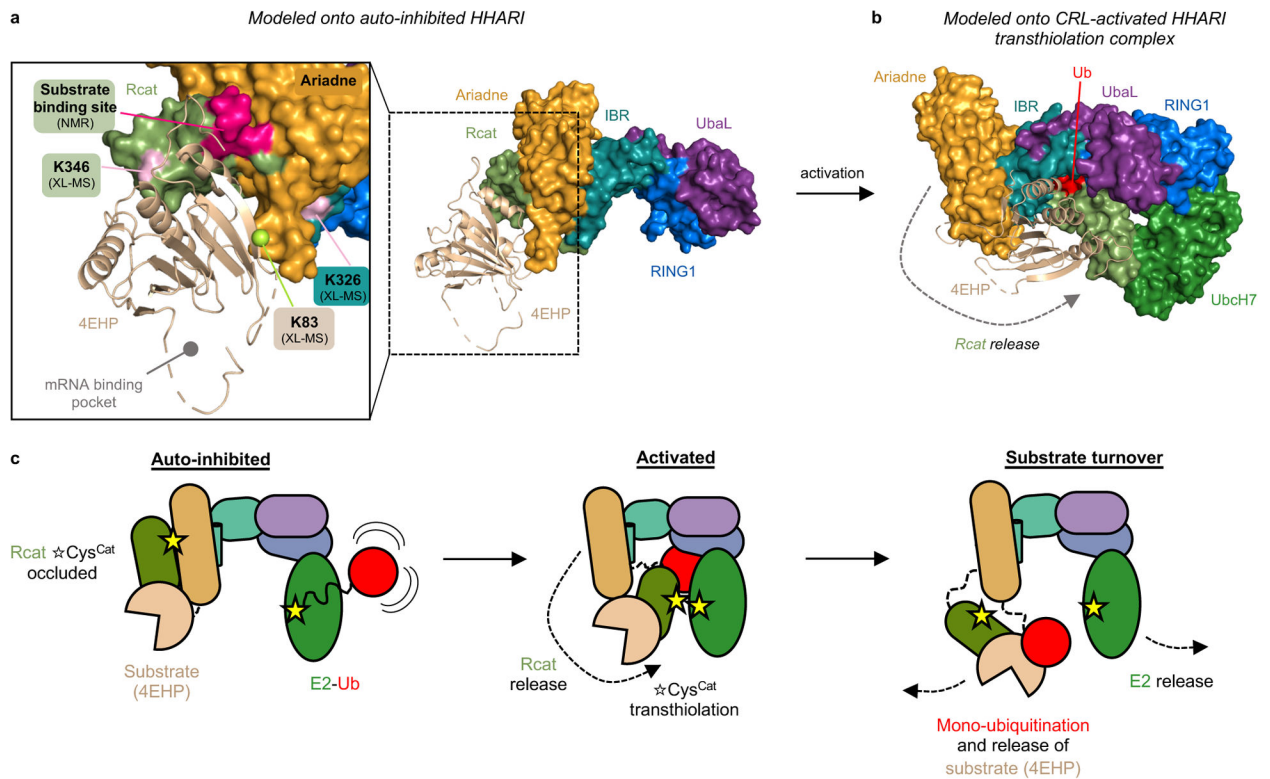


### Figure 7. Modeling of HHARI-4EHP complexes

(A) Visualization of HHARI-4EHP complexes. Auto-inhibited HHARI (PDB: 4KC9) and 4EHP (PDB: 2JGC) are docked with HADDOCK 2.4 software based on NMR and cross-linking results. The docked structure with the lowest HADDOCK score and orientation consistent with HDX results is shown. HHARI and 4EHP are shown as surface and ribbon models respectively. Residues significantly broadened in NMR titrations are shown in dark pink. Cross-linked residues are shown on HHARI (light pink), and 4EHP (light green). (B) Rcat domain of the HADDOCK model shown in (A) is aligned with activated HHARI Rcat (PDB: 7B5L). (C) Model of 4EHP and E2~Ub interactions with auto-inhibited and activated HHARI. Activation untethers 4EHP-bound Rcat from the inhibitory Ariadne domain. Flexible Rcat linkers bring the Rcat-4EHP complex into proximity of RING1-bound E2-Ub (swinging trapeze) to promote transthiolation and substrate ligation. See also Figure S5.

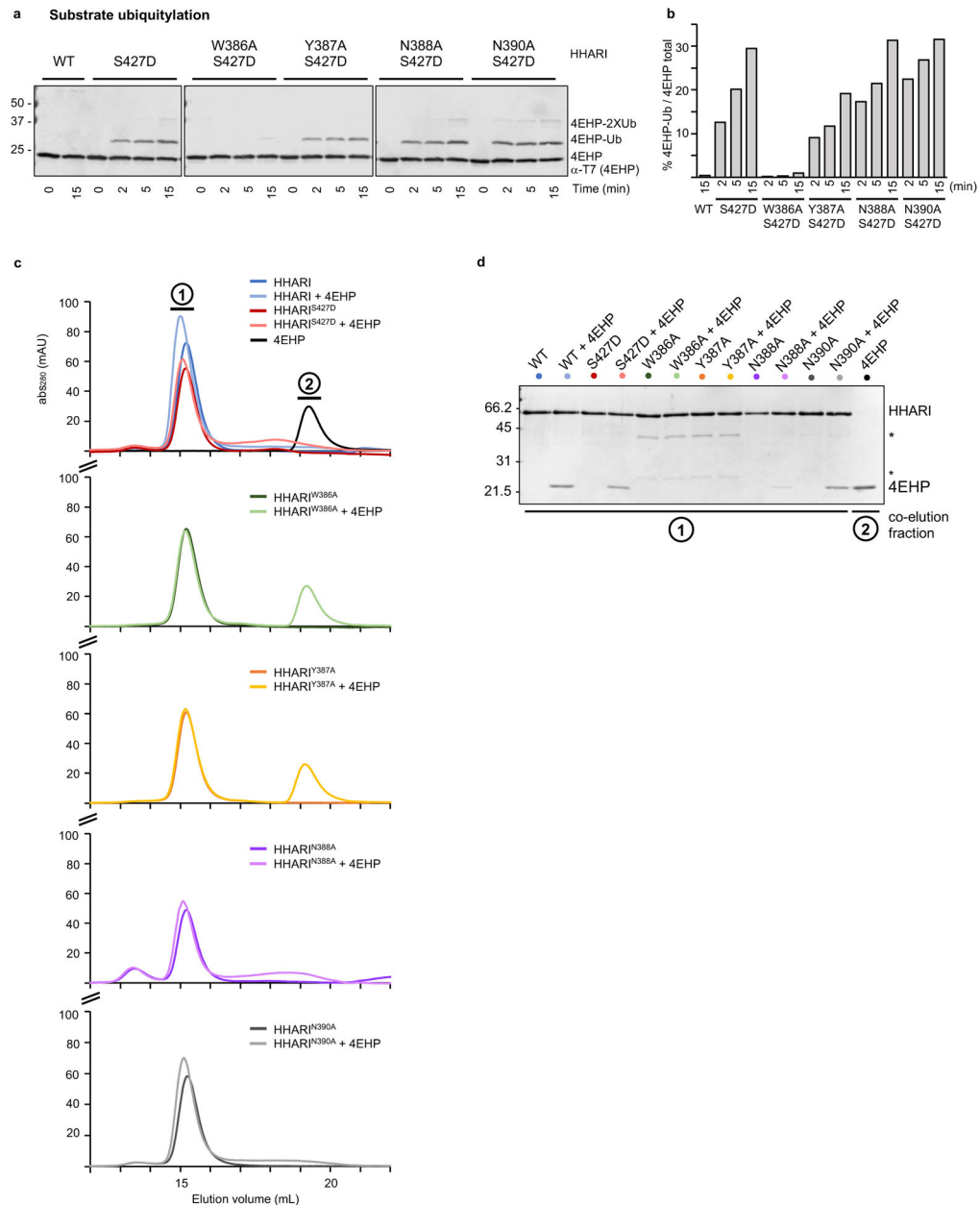


**Figure 8. Rcat surface mutations disrupt 4EHP binding**

(A) 4EHP substrate ubiquitylation assays in response to HHARI Rcat mutations.

Independent western blots are outlined. (B) Ratio of 4EHP-Ub / total 4EHP Alexafluor signal from (A). (C) SEC co-elution profiles of HHARI constructs with 4EHP. Broad absorbance observed for certain samples between the elution volumes for HHARI and 4EHP signifies dissociation of 4EHP from HHARI occurs during the SEC elution. Some preparations of HHARI/HHARI mutants display an early-eluting peak that we attribute to a higher-order species/aggregate. (D) Peak fractions that elute at the position of HHARI (1) or 4EHP alone (2) were analyzed by SDS-PAGE. Sample impurities from HHARI W386A and Y387A purifications are noted with an asterisk.

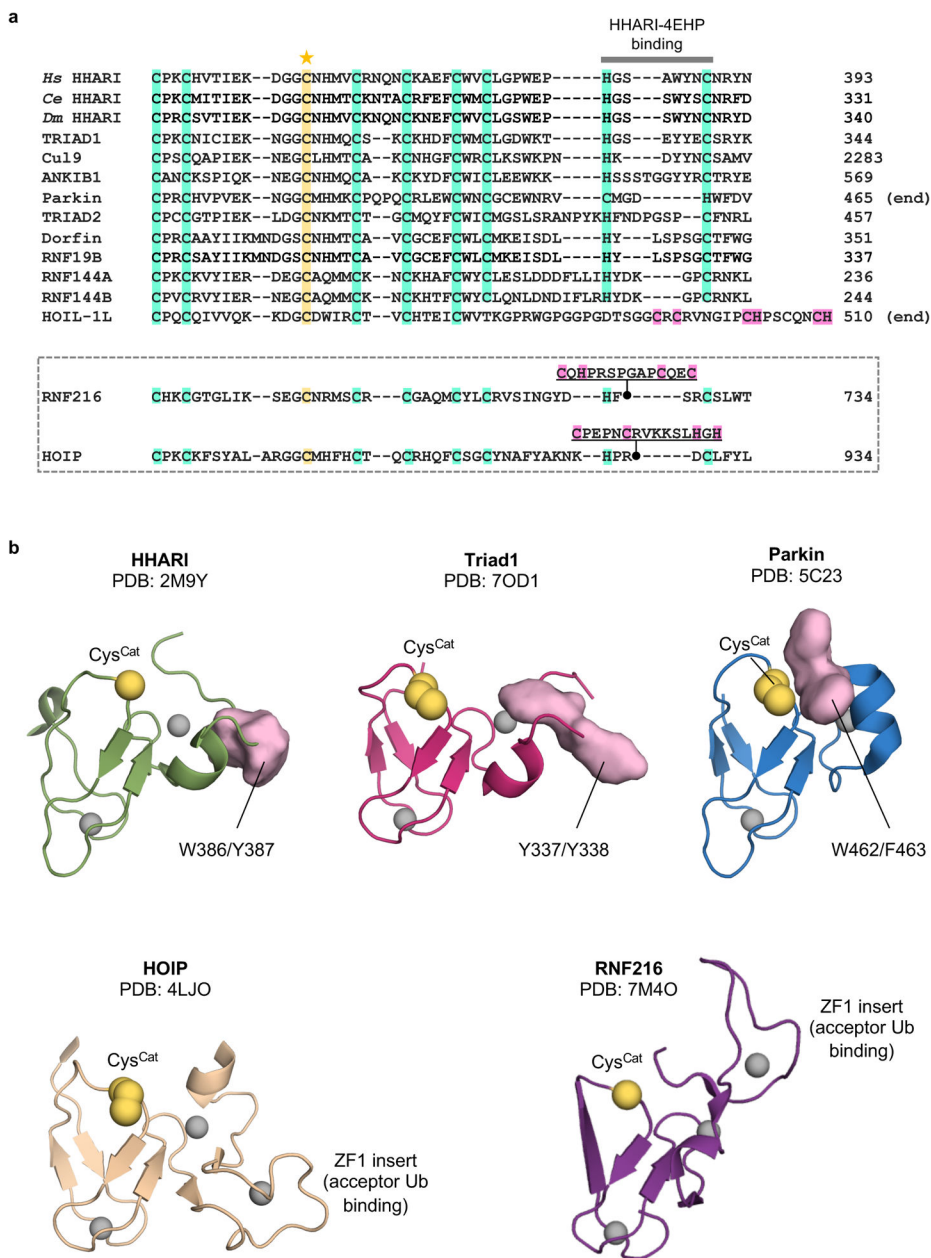


**Figure 9. Conserved features of RBR Rcat domains in putative substrate-binding region.** (A) Multiple sequence alignment of RING-Between-RING Rcat domains, adapted from<sup>2</sup>. Conserved zinc coordinating residues and catalytic cysteines are highlighted in green and yellow, respectively. Additional zinc coordinating residues found in HOIP, HOIL-1, and RNF216 are colored pink. The Rcat region defining the HHARI:4EHP interaction surface identified in this study is noted by a grey bar. (B) Alignment of Rcat domains from atomic structures: HHARI (2M9Y), Triad1 (7OD1), Parkin (5C23), HOIP (4LJO), and RNF216 (7M40). Di-aromatic residues are represented as pink surfaces.

## KEY RESOURCES TABLE

REAGENT or RESOURCE	SOURCE	IDENTIFIER
Antibodies		
Anti-Rabbit DyLight 800	Cell Signaling	5151S
Anti-Mouse Alexa Fluor 680	Invitrogen	A21058
Rabbit polyclonal antiHA antibody	Bethyl Laboratories	A190-108A
Mouse monoclonal anti-T7 antibody	Novagen	69522
Bacterial and Virus Strains		
BL21-Gold (DE3) Competent cells	Agilent Technologies	CAT# 230132
Chemicals, Peptides, and Recombinant Proteins		
Adenosine 5'-triphosphate disodium salt hydrate	Sigma-Aldrich	A2383
[ <sup>15</sup> N]-ammonium chloride	Cambridge Isotope Laboratories, Inc.	NLM-467
Ammonium chloride	JT Baker	0660-01
Zinc chloride	Sigma Aldrich	211273
Deuterium Oxide (D, 99.9%)	Cambridge Isotope Laboratories, Inc.	DLM-4
TCEP	Gold Biotechnology	51805
IPTG	Gold Biotechnology	2481C100
p-Aminobenzamidine-Agarose	Sigma-Aldrich	A8332
Glutathione (reduced)	Sigma Aldrich	G4251
PMSF	Sigma-Aldrich	P7626-100G
cOmplete, EDTA-free Protease Inhibitor Cocktail	Roche	11873580001
DNase	Sigma Aldrich	DN25
RNase	Sigma Aldrich	R5503
Lysozyme	Sigma Aldrich	L6876
LC-MS grade Optima Water	Thermo Fisher Scientific	7732-18-5
DSS	Thermo Fisher Scientific	cat # A39267
Iodoacetamide	Sigma Aldrich	I1149
Sequencing Grade Modified Trypsin	Promega	V5117
PPS Silent Surfactant	Expedeon	21011
ReproSil-Pur 120 C18-AQ 3µm	Dr. Maisch	r13.aq.0003
HHARI WT	This paper	N/A
HHARI F430A/E431A/E503A	This paper	N/A
HHARI S427D	This paper	N/A
HHARI S517D	This paper	N/A
HHARI WT (90-557)	This paper	N/A
HHARI S427D (90-557)	This paper	N/A
HHARI Rcat (325-396)	This paper	N/A
Triad1 WT	This paper	N/A

REAGENT or RESOURCE	SOURCE	IDENTIFIER
Triad1 S378D	This paper	N/A
4EHP WT (45–225)	This paper	N/A
4EHP WT (45–234)	This paper	N/A
UbcH7 WT	This paper	N/A
UbcH7 C86K	This paper	N/A
Uba1	This paper	N/A
Ub WT	This paper	N/A
Ub K0 (K6R, K11R, K27M, K29R, K33R, K48R, K63R)	This paper	N/A
HA-Ub	This paper	N/A
Deposited Data		
Quantification of HHARI/4EHP cross-links in Skyline	This paper	ProteomeXchange ID: PXD030871
Crosslinking-MS raw data files	This paper	ProteomeXchange ID: PXD030849
Recombinant DNA		
pGEX-4T-2-His <sub>6</sub> -GST-TEV-HHARI (WT; F430A/E431A/E503A; S427D; S517D)	This study	N/A
pGEX-6p-1-HHARI res. 90–557 (WT; S427D)	This study	N/A
pGEX-4T-2-His <sub>6</sub> -GST-TEV-HHARI res. 325–396	This study	N/A
pGEX-4T-2-His <sub>6</sub> -GST-TEV-Triad1 (WT; S378D)	This study	N/A
pGEX-6p-1-4EHP res.45–225	This study	N/A
pET28a-His <sub>6</sub> -T7-4EHP res. 45–234	This study	N/A
pET28-UbcH7 (WT)	(Wenzel et al., 2011)	N/A
pET28-UbcH7 (C86K)	This study	N/A
human Uba1	(Wenzel et al., 2011)	N/A
pET15-Ubiquitin (WT)	(Brzovic et al., 2006)	Addgene, Plasmid #12647
pET15-Ubiquitin K0 (K6R, K11R, K27M, K29R, K33R, K48R, K63R)	(Wenzel et al., 2011)	N/A
HA-Ub	(Wenzel et al., 2011)	N/A
Software and Algorithms		
GraphPad Prism version 8	GraphPad Software	<a href="http://www.graphpad.com">http://www.graphpad.com</a>
PyMOL	The PyMOL Molecular Graphics System, Version 2.0 Schrödinger, LLC	<a href="http://www.pymol.org">http://www.pymol.org</a>
HADDOCK 2.4 webserver	(van Zundert et al., 2016)	<a href="https://wenmr.science.uu.nl/haddock2.4Z">https://wenmr.science.uu.nl/haddock2.4Z</a>
TopSpin3.2	Bruker Inc.	<a href="https://www.bruker.com/en/products-and-solutions/mr/nmr-software.html">https://www.bruker.com/en/products-and-solutions/mr/nmr-software.html</a>
NMRPipe	(Delaglio et al., 1995)	<a href="https://www.ibbr.umd.edu/nmrpipe/install.html">https://www.ibbr.umd.edu/nmrpipe/install.html</a>
Protein Prospector	UCSF	<a href="https://prospector.ucsf.edu/prospector/mshome.htm">https://prospector.ucsf.edu/prospector/mshome.htm</a>
MassLynx	Waters Corp	<a href="https://www.waters.com">https://www.waters.com</a>
Driftscope	Waters Corp	<a href="https://www.waters.com">https://www.waters.com</a>
HDExaminer	Sierra Analytics	<a href="http://massspec.com/hdexaminer/">http://massspec.com/hdexaminer/</a>

REAGENT or RESOURCE	SOURCE	IDENTIFIER
ProteoWizard	(Chambers et al., 2012)	<a href="https://proteowizard.sourceforge.io/">https://proteowizard.sourceforge.io/</a>
ProXL	(Riffle et al., 2019)	<a href="https://proxl-ms.org/">https://proxl-ms.org/</a>
Skyline	MacCoss Lab Software	<a href="https://skyline.ms/project/home/software/Skyline/begin.view">https://skyline.ms/project/home/software/Skyline/begin.view</a>
Other		
Superdex 200 resin	GE Healthcare	17104301
Superdex 200 Increase 10/300 GL column	GE Healthcare	28-9909-44
5 mL HisTrap HP column	GE Healthcare	17524801
5 mL SP HP column	GE Healthcare	17115201
PD midiTrap G-25 columns	GE Healthcare	28918008
Glutathione Sepharose 4B resin	GE Healthcare	17075601
Superdex 75 resin	GE Healthcare	17104401

Author Manuscript

Author Manuscript

Author Manuscript

Author Manuscript